The Astrophysical Journal, 794:36 (25pp), 2014 October 10 doi:10.1088/0004-637X/794/1/36

A SPECTROSCOPIC CENSUS IN YOUNG STELLAR REGIONS: THE σ ORIONIS CLUSTER

Jesús Hernández[1], Nuria Calvet[2], Alice Perez[1,3], Cesar Briceño[4], Lorenzo Olguin[5], Maria E. Contreras[6], Lee Hartmann[2], Lori Allen[7], Catherine Espaillat[8], and Ramírez Hernan[1]
[1] Centro de Investigaciones de Astronomía, Apdo. Postal 264, Mérida 5101-A, Venezuela; hernandj@cida.ve
[2] Department of Astronomy, University of Michigan, 500 Church Street, Ann Arbor, MI 48109, USA
[3] Departamento de Física, Universidad de Oriente, Venezuela
[4] Cerro Tololo Interamerican Observatory, Casilla 603, La Serena, Chile
[5] Depto. de Investigación en Física, Universidad de Sonora, Sonora, México
[6] Instituto de Astronomía, Universidad Nacional Autónoma de México, Ensenada, BC, México
[7] National Optical Astronomy Observatory, 950 North Cherry Avenue, Tucson, AZ 85719, USA
[8] Department of Astronomy, Boston University, 725 Commonwealth Avenue, Boston, MA 02215, USA
Received 2014 June 1; accepted 2014 July 31; published 2014 September 22

ABSTRACT

We present a spectroscopic survey of the stellar population of the σ Orionis cluster. We have obtained spectral types for 340 stars. Spectroscopic data for spectral typing come from several spectrographs with similar spectroscopic coverage and resolution. More than half of the stars in our sample are members confirmed by the presence of lithium in absorption, strong Hα in emission or weak gravity-sensitive features. In addition, we have obtained high-resolution ($R \sim 34{,}000$) spectra in the Hα region for 169 stars in the region. Radial velocities were calculated from this data set. The radial velocity distribution for members of the cluster is in agreement with previous work. Analysis of the profile of the Hα line and infrared observations reveals two binary systems or fast rotators that mimic the Hα width expected in stars with accretion disks. On the other hand, there are stars with optically thick disks and narrow Hα profiles not expected in stars with accretion disks. This contribution constitutes the largest homogeneous spectroscopic data set of the σ Orionis cluster to date.

Key words: infrared: stars – open clusters and associations: individual (σ Orionis cluster) – protoplanetary disks – stars: formation – stars: pre-main sequence

Online-only material: color figures, machine-readable tables

1. INTRODUCTION

The σ Orionis cluster located in the Orion OB1 association was first recognized by Garrison (1967) as a group of 15 B-type stars around the massive and multiple system σ Ori AB. Low-mass members of the σ Orionis cluster were reported by Wolk (1996) and Walter et al. (1997), who found more than 80 X-ray sources and spectroscopically identified more than 100 low-mass, pre-main-sequence (PMS) stars. A copious amount of work on this cluster has revealed several hundred low-mass stars and brown dwarfs that could belong to the σ Orionis cluster (see Walter et al. 2008). In the Mayrit catalog, Caballero (2008a) presents a compilation of 241 stars and brown dwarfs that have known features of youth (Li I λ6708 in absorption, strong emission of Hα, infrared excess, X-ray emission, or weak gravity-sensitive features). More than one-third of these stars have disks identified using *Spitzer* photometry (Hernández et al. 2007b, hereafter H07b; Luhman et al. 2008). Recently, deep and wide near infrared surveys have substantially increased the number of substellar candidates of the cluster (e.g., Lodieu et al. 2009; Béjar et al. 2011; Peña Ramírez et al. 2012). The σ Orionis cluster has a dense core extended from the center to a radius of 20′, in which most members are located, and a rarefied halo extended up to 30′ (Caballero 2008b). Other general properties of the σ Orionis cluster are described by Walter et al. (2008).

The σ Orionis cluster is an excellent natural laboratory to study the formation and early evolution of stars and protoplanetary disks in the entire range of stellar masses, from their massive members to the lowest-mass objects such as brown dwarfs and free-floating planets. It has an evolutionary stage at which the beginnings of disk evolution become evident and thus a large diversity of protoplanetary disks is observed (H07b). The age normally used for the cluster is 2–4 Myr (e.g., Zapatero Osorio et al. 2002; Oliveira & van Loon 2004; Franciosini et al. 2006; Sherry et al. 2008; Béjar et al. 2011; Caballero et al. 2012; Rigliaco et al. 2012; Peña Ramírez et al. 2012). Recently, Bell et al. (2013) have derived ages for 13 young stellar groups (including the σ Orionis cluster) that are a factor of two higher than the ages typically adopted in the literature. Regardless of the actual value of the age, a comparison of empirical isochrones reveals that the σ Orionis cluster must be younger than the λ Orionis cluster, the Orion OB1b association, the γ Velorum cluster, and the 25 Ori cluster (Hernández et al. 2008); the age of these groups typically adopted in the literature covers the range from 5 to 10 Myr, and they have consistently smaller protoplanetary disk frequencies than σ Ori.

The σ Orionis cluster is relatively near and the reddening toward the center of the cluster is low ($E(B-V) \lesssim 0.1$ mag; Brown et al. 1994; Béjar et al. 1999, 2004; Sherry et al. 2008). The distance of 352^{+166}_{-85} pc calculated by *Hipparcos* for the central system (σ Ori AB) agrees, within the uncertainties, with the *Hipparcos* distance calculated for the overall population of the stellar subassociation OB1b (439 ± 33; Brown et al. 1998), which is statistically more reliable. This value agrees to the distance of 420 ± 30 estimated by Sherry et al. (2008) from main sequence fitting corrected for the sub-solar metallicity expected in the Orion OB1 association (Cunha et al. 1998; Walter et al. 2008). On the other hand, assuming that σ Ori AB is a double system, Caballero (2008c) estimated a distance of 334^{+25}_{-22} for this object; however, he also estimated a distance of $\sim$385 pc in the case that σ Ori AB was a triple system. Few years later, Simón-Díaz et al. (2011) reported a third

massive star component confirming the σ Ori AB as a triple system (with masses of 19 $M_{\odot}$, 15 $M_{\odot}$, and 9 $M_{\odot}$). Finally, recent interferometric observations of the σ Ori system during periastron in the Center for High Angular Resolution Astronomy with the Michigan Infra-Red Combiner yield a distance of 380.7 $\pm$ 7.1 pc for σ Ori AB (Gail Schaefer and John Monnier 2013, private communication). This value is in agreement with the distance estimated by Caballero (2008c) and within 2σ from the distance reported by Sherry et al. (2008). In this paper, we assume a distance of 385 pc reported by Caballero (2008c).

Regardless of the numerous studies in the σ Orionis cluster, dozens of candidates remain without spectroscopic confirmation of membership (Caballero et al. 2008), and spectroscopically determined stellar characterization exists for only a small fraction of the σ Orionis objects (Rigliaco et al. 2011, 2012; Cody & Hillenbrand 2010). Moreover, spectral types or effective temperatures published for members or candidates of the σ Orionis cluster are obtained from spectroscopic data with different spectral coverage and resolution and applying different methods, which could introduce systematic differences between several samples (e.g., Wolk 1996; Walter et al. 1997; Béjar et al. 1999; Zapatero Osorio et al. 2002; Barrado y Navascués et al. 2003; Scholz & Eislöffel 2004; González Hernández et al. 2008; Caballero 2006; Caballero et al. 2008, 2012; Cody & Hillenbrand 2011; Rigliaco et al. 2012). The spectral type is key for deriving fundamental quantities such as visual extinction, temperature, and luminosity, which in turn allow the determination of stellar radii, masses, and ages. In this contribution, we analyze several sets of spectroscopic data in order to obtain homogeneously spectral types and spectroscopic membership for stars in the σ Orionis cluster. This paper is organized as follows. In Section 2, we describe the observational data and the target selection in the cluster. In Section 3, we discuss results from the low-resolution spectroscopic analysis (Section 3.1), the high-resolution spectroscopic analysis (Section 3.2), memberships based on photometric data and proper motions analysis (Section 3.3), and an overall membership analysis of stars studied in this work (Section 3.4). In Section 4.1, we revisit the disk population of the σ Orionis cluster and we compare our results with the disk census from H07b. In Section 4.2, we discuss the relation between the infrared excesses of disk bearing stars and the accretion properties obtained from high-resolution analysis of the Hα line. Finally, we present our conclusions in Section 5.

2. OBSERVATIONS AND TARGET SELECTION

2.1. Optical Photometry

2.1.1. OSMOS Photometry

We obtained optical photometry ($UBVR_{\rm C}I_{\rm C}$) of the center of the cluster on 2011 December 24 using the Ohio State Multi-Object Spectrograph (OSMOS) on the MDM 2.4 m Hiltner telescope (Stoll et al. 2010; Martini et al. 2011). We obtained two sets of images, one short exposure set (20, 15, 10, 5, and 5 s for U, B, V, $R_{\rm C}$ and $I_{\rm C}$, respectively) and one long exposures set (3 $\times$ 200, 3 $\times$ 200, 3 $\times$ 150, 3 $\times$ 100, and 3 $\times$ 100 s for U, B, V, $R_{\rm C}$, and $I_{\rm C}$, respectively). OSMOS has an all-refractive design that re-images a 20′ diameter field of view onto the 4064 $\times$ 4064 MDM4K CCD with a plate scale of 0.″273 pixel^{-1}. The effective non-vignetted field of view is 18.′5 $\times$ 18.′5. We used 2$\times$2 binning, which gives a final plate scale of 0.″55 pixel^{-1}. The MDM4K CCD is read out using four amplifiers and has a known issue of crosstalk between the four CCD segments of each amplifier. When a CCD pixel is saturated, it creates spurious point sources in corresponding pixels on the other three segments.

Each OSMOS frame was first corrected by overscan using the IDL program proc4k written by Jason Eastman for the Ohio State 4k CCD imager and modified to process OSMOS data. We then performed the basic reduction following the standard procedure using IRAF. We performed aperture photometry for the initial sample (Section 2.2) with the IRAF package APPHOT. The IRAF routine mkapfile was used to determine aperture corrections for each filter. We used Landolt standard fields for photometric calibration in the Johnson–Cousin system (Landolt 2009, 1992). If a star was saturated in the long exposure images, then the short-exposure measurements were used. Non-detections in the combined long exposure images, saturated stars in short exposure images, and photometry affected by bleeding or crosstalk from saturated stars were removed. The saturation limit for the short exposure image is $V \sim 12$ and the limit magnitude for the combined long exposure image is $V \sim 23$.

2.1.2. Additional Photometry

Since OSMOS photometry only covers the central region of the cluster (the dense core), we completed the optical data set used in this paper using Johnson–Cousin photometry from different catalogs.

1. The CIDA Variability Survey of Orion (CVSO; Briceño et al. 2005; Mateu et al. 2012), which has been carried out since 1999 using the Jurgen Stock 1 m Telescope with the QUEST I camera (an array of 4 $\times$ 4 CCD detectors; Baltay et al. 2002) in the Venezuelan National Observatory at Llano del Hato. The region studied in this work is covered almost completely in this multi-epoch survey. Only a small region in the range of declination from $-2.^{\circ}52$ to $-2.^{\circ}44$, corresponding to the gap between CCDs in the QUEST I camera (Vivas et al. 2004; H07b), lacks data. The saturation limit for this survey is $V \sim 13.5$ and the limit magnitude is $V \sim 19.5$.
2. Sherry et al. (2004) presented a $BVR_{\rm C}I_{\rm C}$ survey of 0.89 deg^2 around the σ Orionis cluster. Observations were made with the 0.9 and 1.5 m telescopes at the Cerro Tololo Inter-American Observatory. The reported completeness limit is $V = 18$ within 0.°3 of the σ Ori AB star and $V = 20$ for regions more than 0.°3 from the σ Ori AB star. This catalog includes optical photometry for 234 likely members of the cluster.
3. The Cluster Collaboration's Photometric Catalogs collects photometric data for several young stellar associations and clusters. The catalogs were created using the optimal photometry algorithm described in Naylor (1998) and Naylor et al. (2002). For the σ Orionis cluster, Kenyon et al. (2005) and Mayne et al. (2007) presented $R_{\rm C}I_{\rm C}$ and $BVI_{\rm C}$ photometry, respectively. These data sets were obtained using the Wide Field Camera on the 2.5 m Issac Newton Telescope with the Harris BVR filters and the Sloan i filter. The magnitudes were calibrated using Landolt fields, thus the final photometry is reported in the Johnson–Cousin systems. Sources of the initial sample with optical photometry from these catalogs cover a brightness range from $V \sim 11.5$ to $V \sim 23.5$.
4. The All-sky Compiled Catalogue of 2.5 million stars (ASCC-2.5 V3; Kharchenko & Roeser 2009). This catalog collects B and V Johnson photometry mainly from

Hipparcos–Tycho family catalogs. The limiting magnitude is $V \sim 12$–14, although the completeness limit (to 90%) is $V \sim 10.5$ mag. We augmented the V, B optical data set toward the brightest objects using the ASCC-2.5 V3 catalog.

Using stars in common between the different catalogs and OSMOS photometry, we find (after 3σ clipping) that the V-band measurements are comparable within 0.5%, 1.6%, and 1.7% for the CVSO, Sherry et al. (2008), and the Cluster Collaboration Photometric Catalog, respectively. We do not have enough common stars between OSMOS data and Kharchenko & Roeser (2009) catalog to do this comparison.

2.2. Initial Sample

The initial sample in this study includes all Two Micron All Sky Survey (2MASS) sources (4659 sources; Cutri et al. 2003) in a region of $48' \times 48'$ centered at R.A. $= 84.^{\circ}7$ and decl. $= -2.^{\circ}6$. This region covers the field studied in H07b using the four channels of the InfraRed Array Camera (IRAC; Fazio et al. 2004). The 2MASS catalog is complete down to $J < 15.8$, which includes stars beyond the substellar limit expected for the σ Orionis cluster (e.g., $J \sim 14.6$; H07b). We compared sources from the 2MASS catalog and from the United Kingdom Infrared Telescope (UKIRT) Infrared Deep Sky Survey (UKIDSS; Lawrence et al. 2007, 2013). When 2MASS sources have poor photometric quality flag ("U," "F," or "E") for the J magnitude, we use photometric measurements reported in the UKIDSS catalog.

Out of 31 UKIDSS sources with $J < 15.8$ and without 2MASS counterparts, 10 sources are galaxies based on the profile classification of UKIDSS and 16 sources are close visual binaries not resolved in 2MASS images (2MASS reports photometry only for the brightest companion). From the remaining five sources, four stars are background candidates and only one star is a photometric member based on its location in the Z versus $Z-J$ color–magnitude diagram (Lodieu et al. 2009). This star has an optically thick disk (SO 566; H07b) and the non-detection in 2MASS images suggests large variability (variability amplitude in J band $\gtrsim 2.7$). The star SO 566 was added to the initial sample of 4659 2MASS sources. Finally, there are four additional sources studied in H07b without 2MASS counterpart (SO 406, SO 336, SO 361, and SO 950). Since all these sources are fainter ($J > 17.9$ in UKIDSS) than the 2MASS completeness limit, they were not included in this study.

2.2.1. 2MASS Sources without Optical Photometry

Out of 4660 sources in the initial sample, 4444 sources (95.4%) have optical counterparts (at least in filter V). Out of 216 sources without optical photometry, 160 stars are fainter than the completeness limit of 2MASS catalog and were not included in this study. Out of 56 stars brighter than the completeness limit of 2MASS catalog, 52 stars have photometric memberships reported by Lodieu et al. (2009) and 4 stars are brighter than the Z-band limit used by Lodieu et al. (2009) for their membership criteria. They found 14 photometric candidates, 35 background candidates, and 3 Galaxies based on the stellar profile classification and color–magnitude diagrams. Three of these photometric candidates are studied in Section 3.1, the remaining 11 sources are detailed in the Appendix.

2.3. Compilation of Known Members

We compiled lists of spectroscopically confirmed members of the σ Orionis cluster on the basis that they exhibit Li I λ6708 in absorption or they have radial velocities (RVs) expected for the kinematic properties of the cluster (hereafter "spectroscopic known members").

Using RV measurements, Jeffries et al. (2006) showed that young stars located in the general region of the cluster consist of two stellar groups kinematically separated by 7 km s^{-1} in RV and with different mean ages and distances. One group has RVs from 27 km s^{-1} to 35 km s^{-1}, which is consistent with the RV of the central star σ Ori AB (29.5 km s^{-1}; Kharchenko et al. 2007). The other group has RVs from 20 km s^{-1} to 27 km s^{-1} and could be in front of the first group and could have a median age and distance similar to older stellar groups associated with the sparser Orion OB1a subassociation (age ~ 10 Myr; distance $\sim$326; Briceño et al. 2007). This older and kinematically distinct stellar population (hereafter "the sparser stellar population") is located to the northwest of the central system and more difficult to detect in RV distributions of stars located near the center of the cluster (Sacco et al. 2008). Using the limit defined by Jeffries et al. (2006), we included in our study 162 kinematic members of the σ Orionis cluster, with RV between 27 and 35 km s^{-1}, from Zapatero Osorio et al. (2002), Kenyon et al. (2005), Caballero (2006), Burningham et al. (2005), Maxted et al. (2008), Sacco et al. (2008), and González Hernández et al. (2008).

We also included as spectroscopic known members, 181 stars with Li I λ6708 in absorption from Wolk (1996), Alcalá et al. (1996), Zapatero Osorio et al. (2002), Muzerolle et al. (2003), Barrado y Navascués et al. (2003), Andrews et al. (2004), Kenyon et al. (2005), Caballero (2006), Caballero et al. (2006, 2012), González Hernández et al. (2008), and Sacco et al. (2008). Since the presence of lithium is an indicator of youth in late-type stars, our selection includes stars with reported spectral types K or M. Our list includes all late-type stars with Li I λ6708 in absorption compiled in the Mayrit Catalog (Caballero 2008a).

Additionally, we have compiled 168 X-ray sources reported by Caballero (2008a), Skinner et al. (2008), López-Santiago & Caballero (2008), Caballero et al. (2009, 2010), or X-ray sources in the *XMM-Newton* Serendipitous Source Catalog 2XMMi-DR3 (XMM-SSC, 2010) with source detection likelihoods (srcML) larger than eight (sources with scrML < 8 may be spurious). Since young stars are strong X-ray emitters, likely members of the σ Orionis clusters are X-ray stellar sources located above the zero-age main sequence (ZAMS).

Finally, another indicator of youth is the infrared excess present when stars are surrounded by circumstellar disks. Using *Spitzer Space Telescope* observations, we reported 114 photometric candidates with infrared excesses (H07b).

Youth indicators based on the presence of Li I λ6708 in absorption, X-ray observations and infrared excesses do not discriminate interlopers from the sparser stellar population. Regardless of this expected contamination, we define the sample of known likely members (hereafter "known members") compiling kinematic members based on RVs, stars with Li I λ6708 in absorption, X-ray sources above the ZAMS and stars with infrared excesses. Table 1 shows information about the known member sample.

2.4. Target Selection

Using the photometric data compiled in Sections 2.1.1 and 2.1.2, we selected photometric candidates of the σ Orionis cluster. Although we have V, R_C, I_C, and J magnitudes for most stars in the initial sample, we use the $V-J$ color because is the most complete for our sample and it has the greatest color leverage for constraining PMS populations.

Table 1
Compiled Membership Information of the σ Orionis Cluster

Name H07	2massID	R.A. (deg)	Decl. (deg)	Disk Type	Li I Ref.	RV Ref.	X-Ray Ref.
SO27	05372306-0232465	84.346086	−2.546276	III	···	···	19
SO59	05372806-0236065	84.366955	−2.60182	III	···	···	16,19
SO60	05372831-0224182	84.367989	−2.40506	III	···	···	16,19
SO73	05373094-0223427	84.378949	−2.395214	II	···	···	19
SO77	05373153-0224269	84.381401	−2.407489	III	6	···	16,19
SO107	05373514-0226577	84.396435	−2.44937	III	···	···	19
SO116	05373648-0241567	84.40202	−2.699093	III	3,5,12	···	···
SO762	05385060-0242429	84.710859	−2.711918	II	5	5,13	···
SO765	05385077-0236267	84.711581	−2.607432	III	5,8	5,8	18
SO976	05391699-0241171	84.820833	−2.688091	III	···	···	14,18,19
SO1185	05394340-0253230	84.930841	−2.889736	III	···	5	···
···	05381741-0240242	84.572574	−2.673413	···	2,3,5	13	···
···	05382557-0248370	84.606573	−2.810284	···	2,3	···	···
··· [a]	05390756-0212145	84.78150	−2.204030	···	···	···	···
···	05390893-0257049	84.787241	−2.951387	···	6	···	···
···	05402018-0226082	85.084123	−2.435633	···	···	···	14
···	05402076-0230299	85.086534	−2.508313	···	···	···	14
···	05402256-0233469	85.094019	−2.56303	···	6	7	14
···	05402301-0236100	85.095882	−2.6028	···	6	13	···

Notes.
Disk type: III = diskless, II = thick disk, I = class I, EV = evolved disk, TD = transition disk, DD = Debris disk.
[a] Strong Hα line and Accretion disk (Scholz & Eislöffel 2004; Scholz et al. 2009).
[b] Strong Hα line and Accretion disk (Caballero et al. 2008).
References. (1) Wolk 1996; (2) Zapatero Osorio et al. 2002; (3) Barrado y Navascués et al. 2003; (4) Andrews et al. 2004; (5) Kenyon et al. 2005; (6) Caballero 2006; (7) González Hernández et al. 2008; (8) Sacco et al. 2008; (9) Caballero et al. 2012; (10) Alcalá et al. 1996; (11) Caballero et al. 2006; (12) Muzerolle et al. 2003; (13) Maxted et al. 2008; (14) Caballero 2008a; (15) Skinner et al. 2008; (16) López-Santiago & Caballero 2008; (17) Caballero et al. 2009; (18) Caballero 2010; (19) XMM-SSC, 2010); (20) Burningham et al. 2005.

(This table is available in its entirety in a machine-readable form in the online journal. A portion is shown here for guidance regarding its form and content.)

Figure 1 shows the color–magnitude diagram V versus $V-J$ for sources in the initial sample with optical counterparts. We have estimated an empirical isochrone as the location of known members compiled in Section 2.3; stars with infrared excesses, young stars confirmed using the presence of Li I λ6708 in absorption, kinematic members confirmed using RVs, and X-ray sources above the ZAMS (Siess et al. 2000) located at 385 pc (Caballero 2008c). The empirical isochrone in Figure 1 was estimated using the median $V-J$ color of the known members for 1 mag bins in the V band. Standard deviations (σ) were calculated using the differences between the observed colors and the expected colors from the empirical isochrone. We fitted two straight lines to the points represented by the empirical isochrone color + 3σ and by the empirical isochrone color −3σ. Photometric candidates are stars that fall between these lines (Hernández et al. 2008, 2010).

Our photometric sample includes the photometric candidates reported in H07b using a more limited optical photometric data set. The present sample is larger because we have included an updated version of the CVSO catalog (Mateu et al. 2012), photometry from the cluster collaboration, and the new OSMOS photometry described in Section 2.1.1.

Out of 255 spectroscopic known members and disk bearing candidates, 249 stars are located in the photometric candidates region. Based on this, we lose about 2.4% of known members of the σ Orionis cluster with our photometric selection. Since targets for spectroscopic follow up generally are selected using photometric cuts, the exclusion percentage of know members could be a lower limit of the percentage of actual members excluded from our photometric selection. On the other hand, Burningham et al. (2005) found that photometric selection cuts do not miss significant numbers of bona-fide members of the σ Orionis cluster and thus the percentage of actual member excluded by our photometric selection can not be much higher than ∼2.4%. Since our photometric criteria to select candidates is conservative, contamination by background stars is present in the entire color range. At a color $V-J \sim 1.5$, where a branch of old field stars crosses the PMS of the σ Orionis cluster, the expected contamination level by non-members of the cluster is quite high (e.g., Hernández et al. 2008). Table 2 includes optical magnitudes for the photometric candidates and for the known members not located in the photometric candidates region.

2.5. Low-resolution Spectroscopy

Optical low-resolution spectra is a fundamental tool to identify and characterize young stars by using indicators as the presence of lithium in absorption, strong Hα in emission or weak gravity-sensitive features. We have obtained low-resolution spectra for 340 stars located in the σ Orionis cluster. This spectroscopic data comes from several spectrographs with similar spectral coverage and resolution (see Table 3). Targets for spectroscopic followup were selected mainly from the sample of photometric members with infrared excesses or the sample of photometric members with X-ray counterparts. Except for observations obtained using the Hectospec multifibers spectrograph, target selection includes stars with V magnitude brighter than 16.5. Using the 3 Myr isochrone from Siess et al. (2000)

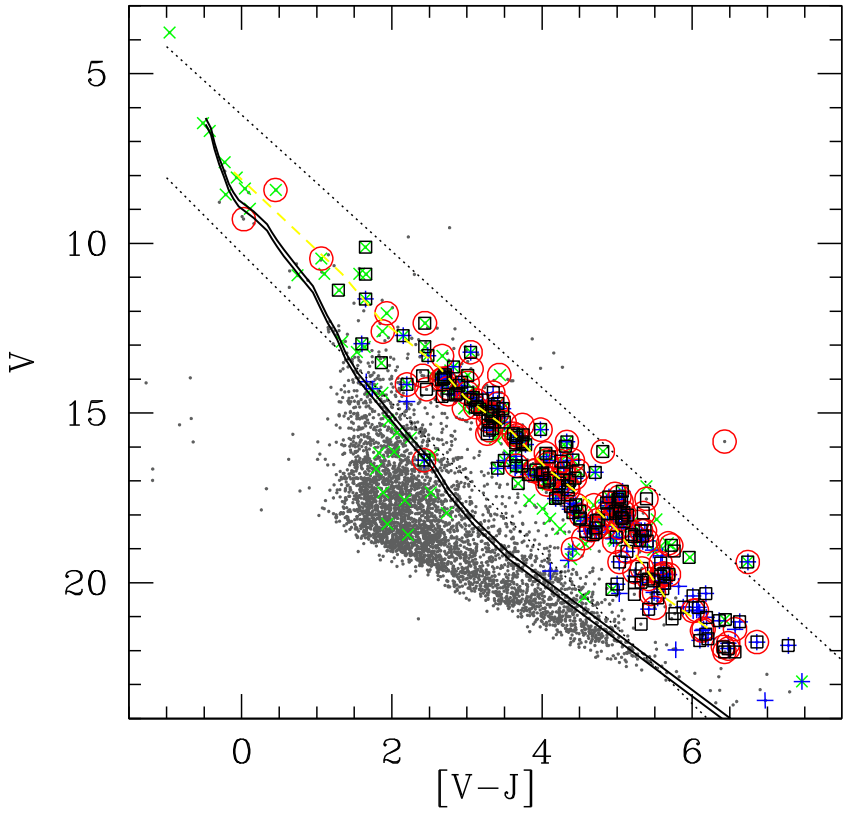

Figure 1. V vs. $V-J$ color–magnitude diagram, illustrating the selection of photometric members of the σ Orionis cluster. Open red circles represent stars with infrared excesses (H07b). Open squares represent young stars confirmed using the presence of Li I λ6708 in absorption. Plus signs represent kinematic members confirmed using RVs. Symbols "x" represent X-ray sources. Likely members are X-ray sources above the zero-age main sequence (ZAMS). The dashed line represents the empirical isochrone estimated from the median colors of the known members sample. Dotted lines limit the region where members are expected to fall (photometric member region). By comparison, the ZAMS from Siess et al. (2000) was plotted assuming a distance of 420 pc (Sherry et al. 2008) and 385 pc (Caballero 2008c).
(A color version of this figure is available in the online journal.)

and assuming a distance of 385 pc (Caballero 2008c) without reddening, this limit corresponds to stars of spectral type M3 or earlier ($M_* > 0.35\ M_\odot$).

2.5.1. Hectospec

We obtained low-resolution spectra with the fiber-fed multi-object Hectospec instrument mounted on the 6.5 m Telescope of the MMT Observatory (MMTO). Hectospec has 300 fibers that can be placed within a 1° diameter field. Each fiber subtends 1.″5 on the sky (Fabricant et al. 2005). The observations were taken with 270 line mm^{-1} grating, providing ∼6 Å resolution and spectral coverage of 3650–9200 Å. The Hectospec data were reduced through the standard Hectospec data reduction pipeline (Mink et al. 2007). This pipeline assumes that the sky background does not vary significantly with position on the sky and uses combined sky fibers (fibers that point to empty portions of the sky) to correct for the sky background. In general, the σ Orionis cluster has a smooth background. However, there are some targets located in regions with variable sky background and therefore their spectra could have bad estimates of nebular lines. We have identified 16 stars with bad sky subtraction and for these stars we did not report measurements of the Hα line. One observation was obtained on the night of 2006 October 11, which provided spectra for 160 photometric candidates and 56 additional stars in the field.

2.5.2. FAST

We obtained low-resolution spectra for 46 photometric candidates using the 1.5 m telescope of the Fred Lawrence Whipple Observatory with the FAST spectrograph (Fabricant et al. 1998), equipped with the Loral 512 × 2688 CCD. The spectrograph was set up in the standard configuration used for FAST COMBO projects, a 300 groove mm^{-1} grating and a 3″ wide slit. This combination offers 3400 Å of spectral coverage centered at 5500 Å, with a resolution of 6 Å. These data were observed as part of the program "Orion PMS Candidates" (112; Briceño et al. 2005, 2007). The spectra were reduced at the Harvard-Smithsonian Center for Astrophysics using software developed specifically for FAST COMBO observations. Additionally, we have five stars collected as part of the FAST program "Ae/Be stars in OB associations" (89; Hernández et al. 2005). Finally, using the FAST Public Archive,[9] we have collected spectra for 19 additional stars observed as part of different programs.

2.5.3. OSU-CCDS

Low-resolution, long slit-spectra were obtained for 36 photometric candidates using the 1.3 m McGraw-Hill Telescope of the MDM Observatory (MDMO) with the OSU (Ohio State University) Boller & Chivens CCD spectrograph (OSU-CCDS) equipped with the Loral 1200 × 800 CCD. We used the 158 grooves per mm grating centered at 5300 Å along with a 1″ slit width. This configuration provides an effective resolution of 6.5 Å with 3400 Å of spectral coverage (the nominal resolution of 4.1 Å provides spectra under sampled at the 1.3 m telescope). Observation were obtained on the nights of 2011 December 16 and 17. Processing of the raw frames and calibration of the

[9] http://tdc-www.harvard.edu/cgi-bin/arc/fsearch

Table 2
Photometric Candidates

Name H07	2massID	RAJ2000 (deg)	DECJ2000 (deg)	U (mag)	B (mag)	V (mag)	R (mag)	I (mag)	J (mag)	Ref.
...	05371360-0229293	84.30668	−2.49147	...	16.48 ± 0.02	15.19 ± 0.00	...	13.52 ± 0.01	12.25 ± 0.04	CLC
...	05371373-0258190[c]	84.30724	−2.97196	...	21.53 ± 0.64	21.08 ± 0.02	19.74 ± 0.02	17.98 ± 0.05	16.11 ± 0.11	CLC
...	05371407-0221089	84.30863	−2.35249	...	...	13.39 ± 0.02	...	...	11.18 ± 0.02	CVSO
...	05372254-0259363	84.34395	−2.99343	...	...	15.06 ± 0.01	14.13 ± 0.01	13.15 ± 0.01	11.73 ± 0.02	S04
SO77	05373153-0224269	84.38140	−2.40749	...	17.32 ± 0.02	15.85 ± 0.01	14.72 ± 0.01	13.45 ± 0.01	12.11 ± 0.03	S04
SO189	05374924-0253118	84.45518	−2.88662	...	...	18.04 ± 0.07	16.94 ± 0.02	...	14.44 ± 0.04	CVSO
SO199	05374981-0246032	84.45757	−2.76756	...	...	13.74 ± 0.02	...	...	11.69 ± 0.03	CVSO
SO247	05375486-0241092	84.47860	−2.68590	...	19.68 ± 0.18	18.34 ± 0.09	17.14 ± 0.06	15.43 ± 0.03	13.50 ± 0.03	S04
SO389	05381223-0218124	84.55097	−2.30345	...	16.79 ± 0.02	15.39 ± 0.01	14.51 ± 0.01	13.71 ± 0.01	12.66 ± 0.00[a]	CLC
SO411	05381412-0215597	84.55884	−2.26660	...	10.93 ± 0.06	10.45 ± 0.06	...	...	9.39 ± 0.02	K09
SO563	05383157-0235148	84.63158	−2.58746	18.19 ± 0.18	17.17 ± 0.02	15.85 ± 0.01	14.88 ± 0.01	13.77 ± 0.01	11.52 ± 0.03	OS
SO567	05383243-0251215	84.63514	−2.85597	...	14.20 ± 0.01	13.34 ± 0.01	...	12.24 ± 0.01	11.60 ± 0.03	CLC
SO706	05384480-0233576	84.68668	−2.56601	14.82 ± 0.02	13.73 ± 0.00	12.49 ± 0.00	11.77 ± 0.00	11.11 ± 0.00	10.01 ± 0.03	OS
...	05384503-0258340	84.68766	−2.97612	...	21.78 ± 0.84	19.61 ± 0.01	18.24 ± 0.01	16.75 ± 0.01	15.20 ± 0.04	CLC
SO739	05384818-0244007	84.70078	−2.73355	21.27 ± 0.49	21.43 ± 0.09	19.76 ± 0.02	18.11 ± 0.01	16.13 ± 0.01	14.07 ± 0.03	OS
SO927	05391151-0231065	84.79798	−2.51849	16.75 ± 0.07	16.98 ± 0.02	15.66 ± 0.01	14.64 ± 0.01	13.56 ± 0.01	11.99 ± 0.03	OS
SO929	05391163-0236028	84.79846	−2.60080	17.04 ± 0.07	15.82 ± 0.01	14.47 ± 0.00	13.61 ± 0.00	12.75 ± 0.00	11.62 ± 0.03	OS
SO947	05391453-0219367	84.81056	−2.32687	...	17.33 ± 0.02	15.90 ± 0.02	14.83 ± 0.02	13.60 ± 0.02	12.16 ± 0.03	S04
SO1081	05393056-0238270[c]	84.87733	−2.64084	...	19.36 ± 0.13	17.82 ± 0.05	16.61 ± 0.03	15.21 ± 0.02	13.81 ± 0.03	S04
SO1224	05394891-0229110[c]	84.95381	−2.48641	...	19.02 ± 0.10	17.34 ± 0.03	16.24 ± 0.02	14.70 ± 0.01	13.28 ± 0.03	S04
...	05400405-0255375	85.01689	−2.92711	...	...	17.46 ± 0.05	16.40 ± 0.02	15.18 ± 0.02	14.07 ± 0.03	CVSO
...	05402378-0228261	85.09912	−2.47394	...	...	17.78 ± 0.05	16.74 ± 0.02	...	13.86 ± 0.04	CVSO

Notes.
[a] J magnitude from UKIDSS.
[b] Known members not selected as photometric candidates.
[c] Sources labeled as galaxies by Lawrence et al. (2013).
References. OSMOS (OS; Section 2.1.1); CIDA Variability Survey of Orion (CVSO; Briceño et al. 2005); Sherry et al. (2004; S04); Cluster Collaboration (CLC; Kenyon et al. 2005; Mayne et al. 2007); Kharchenko & Roeser (2009; K09).

(This table is available in its entirety in a machine-readable form in the online journal. A portion is shown here for guidance regarding its form and content.)

Table 3
Low Resolution Spectrographs

Observatory	Telescope meters	Spectrograph	Resolution at Hα Å	REF	Spectral Coverage Å
MMTO	6.5	Hectospec (H)	6	Fabricant et al. (2005)	3650–9200
FLWO	1.5	FAST (F)	6	Fabricant et al. (1998)	3800–7200
MDMO	1.3	OSU-CCDS (O)	6.5	Measured with arc lines	3900–7300
OAN-SPM	2.1	Boller & Chiven (S)	5.5	Measured with arc lines	3900–7200
Guillermo-Haro	2.1	Boller & Chiven (C)	10	Measured with arc lines	4100–7300

spectra were carried out following standard procedures using the IRAF packages twodspec and onedspec.

2.5.4. Boller and Chivens, SPM

Low-resolution, long-slit spectra were obtained with the Boller & Chivens spectrograph mounted on the 2.1 m telescope at the San Pedro Martir Observatory (OAN-SPM)[10] during three observing runs: 2011 October 28–30, 2012 October 18–21, and 2013 January 12–14. A Marconi CCD (13.5 μm pixel^{-1}) with 2k × 2k pixel array was used as detector. We have used a 400 lines mm^{-1} dispersion grating along with a 2″ slit width, giving a spectral resolution of ∼6 Å. Spectra reduction was carried out following standard procedures in XVISTA.[11] In order to eliminate cosmic rays from our spectra, we have obtained three spectra for each star and combined them to get a median individual spectrum. A total of 34 photometric candidates were observed with this instrument.

2.5.5. Boller and Chivens, Cananea

A set of low-resolution, long-slit spectra was obtained with the Boller & Chivens spectrograph mounted on the 2.1 m telescope at the Observatorio Astrofisico Guillermo Haro (Cananea, Mexico),[12] during the nights of 2012 December 1–4. A SITe CCD with 1k × 1k pixels of 24 microns was used as a detector. We have used a 150 lines mm^{-1} dispersion grating and a slit width of 2″, giving a spectral resolution of ∼10 Å. Observing strategy and spectra reduction were the same as described in Section 2.5.4. A total of 27 photometric candidates were observed with this instrument.

[10] The Observatorio Astronómico Nacional at San Pedro Martir (OAN-SPM) is operated by the Instituto de Astronomía of the Universidad Nacional Autónoma de México.
[11] XVISTA was originally developed as Lick Observatory Vista. It is currently maintained by Jon Holtzman at New Mexico State University and is available at http://ganymede.nmsu.edu/holtz/xvista.
[12] The Observatorio Astrofísico Guillermo Haro (OAGH) is operated by Instituto Nacional de Astrofísica Optica y Electronica (INAOE).

2.6. High-resolution Spectroscopy

We obtained high-resolution spectra of a subset of candidates of the σ Orionis cluster using the Hectochelle fiber-fed multiobject echelle spectrograph mounted on the 6.5 m Telescope of the MMTO. Hectochelle can record up to 240 high-resolution spectra simultaneously in a 1° circular field. Each fiber subtends 1.″5 on the sky (Szentgyorgyi et al. 2011). We use the order-sorting filter OB26 that provides a resolution of $R \sim 34{,}000$ with 180 Å of spectral coverage centered at 6625 Å. In spite of the fact that the order-sorting filter OB26 is not optimal for RV measurements (Fűrész et al. 2008), the spectral coverage of this filter allows us to analyze the Hα profile and the Li I λ6708 line to identify young stars, accretors, and non-accretors.

One Hectochelle field was obtained on the night of 2007 February 27 that provides high-resolution spectra for 134 photometric candidates and 8 additional stars in the region studied in this work. The data were reduced using an automated IRAF pipeline developed by G. Furesz, which utilizes the standard spectral reduction procedures using IRAF and the tasks available under the packages mscred and specred. A more detailed description of Hectochelle data reduction can be found in Sicilia-Aguilar et al. (2006).

3. SPECTRAL TYPES AND MEMBERSHIP

3.1. Spectral Analysis, Youth Features, and Reddening Estimates

Spectral types were derived applying the SPTCLASS code on the sample of stars with low-resolution spectra (Section 2.5). SPTCLASS is a semi-automatic spectral analyzing program that uses empirical relations between spectral type and equivalent widths (EWs) to classify and characterize stars based on selected features.[13] For spectral typing, it has three schemes optimized for different mass ranges (K5 or later, from late F to early K, and F5 or earlier), which use different sets of spectroscopic features (Hernández et al. 2004; Sicilia-Aguilar et al. 2005; Downes et al. 2008). The user has to manually choose the best scheme for each star based on the prominent features in the spectrum and the consistency of several spectral indices. The EW for each spectral feature is obtained by measuring the decrease in flux due to photospheric absorption line from the continuum that is expected when interpolating between two adjacent bands. The spectral features measured by this procedure are largely insensitive to reddening and the signal-to-noise ratio (S/N) of the spectra (as long as we have enough S/N to detect the spectral feature). Moreover, spectral types obtained by SPTCLASS are largely independent of luminosity because most of the indices selected are not sensitive to the surface gravity of the star (Hernández et al. 2004). However, SPTCLASS does not take into account the effect on the lines of the hot continuum emission produced by the accretion shocks. This continuum emission makes the photospheric absorption lines appear weaker and for K-type and M-type highly veiled stars the SPTCLASS outputs should be considered as the earliest spectral-type limits (Hsu et al. 2012). SPTCLASS is unable to give spectral types for highly veiled stars earlier than K-type (e.g., continuum stars in Hernández et al. 2004). In Table 4, we report spectral types for the sample observed in Section 2.5.

In Figure 2, we compare spectral types derived in this work with those published previously from selected works (Wolk 1996; Houk & Swift 1999; Zapatero Osorio et al. 2002; Caballero 2006; Caballero et al. 2012; Rigliaco et al. 2012). Additionally, our spectral types were compared with spectral types compiled in the SIMBAD[14] database from different authors (Cohen & Kuhi 1979; Nesterov et al. 1995; Houk & Swift 1999; Zapatero Osorio et al. 2002; Barrado y Navascués et al. 2003; Muzerolle et al. 2003; Hernández et al. 2005; Briceño et al. 2005; Oliveira et al. 2006; Caballero et al. 2006, 2010, 2012; Gatti et al. 2008; Sherry et al. 2008; Skinner et al. 2008; Renson & Manfroid 2009; Nazé 2009; Cody & Hillenbrand 2010; Townsend et al. 2010; Rigliaco et al. 2011, 2012). Most spectroscopic studies of the σ Orionis cluster have derived spectral types for low-mass stars and very low-mass stars (spectral types K5 or later). Thus, in Figure 2 we have few points of comparison in the solar-type range (from F to early K). In general, and with the exception of Wolk (1996), spectral types reported previously by other authors agree within the uncertainties with spectral types calculated using SPTCLASS. Wolk (1996) used absorption line ratios of Ca I lines (λ6122, λ6162, and λ6494) and Fe I lines (λ6103, λ6200, and λ6574) as indicators of spectral types. The spectral type dependencies of these indicators are weak for stars with spectral types early K or earlier. Additionally, the spectroscopic data set of Wolk (1996) have poor S/N, which severely affects the measurements (Zapatero Osorio et al. 2002). A subset of the stars studied by Wolk (1996) were observed by Zapatero Osorio et al. (2002). Their spectral types, based on the measurements of molecular bands like TiO and CaH, match our determinations. On the other hand, Caballero (2006) used indices based on the EW of some lines (Fe I λ6400, Ca I λ6439, Ca I λ6450, Ca I λ6462, and Ca I λ6717) to estimate spectral types. The spectral type dependencies of these indices are very weak in the spectral type range from G0 to K0, where we observe larger discrepancies between our spectral types and the spectral types reported by Caballero (2006).

EWs of Li I λ6708 and Hα lines were measured using the interactive mode of SPTCLASS in which two adjacent continuum points must be manually selected on the spectra to fit a Gaussian line to the feature.[15] We find that the typical uncertainties of EWs measured in this way are ~10%. In Table 4, we assign a flag to each star based on the presence of Li I λ6708 in absorption: "2" means that the star has Li I λ6708 in absorption; "1" means that there are doubts about the measurement of Li I, generally, due to low S/N of the spectra; and "0" means that Li I λ6708 is not present in the spectra.

Based on the EW of Hα and the criterion defined by Barrado y Navascués et al. (2003) to distinguish between accretors and non-accretors for stars with spectral type G5 or later, in Table 4, we classify stars into different groups: accretors (Acr), non-accretors (nAcr), and stars in which uncertainties for EWs of Hα and spectral types fall on the limit between accretors and non-accretors (Acr?). We also have identified stars with spectral types earlier than G5 with Hα in emission (ET_{em}) and with Hα in absorption (E_{abs}). Figure 3 shows the relation between the EW of Hα and the spectral type. In order to plot our data in a logarithmic scale, EWs of Hα have been shifted by 10 units (the dotted line is the limit between absorption and emission of Hα). Solid line delimits the area for accretors and non-accretor stars based on the EWs of Hα emission line (Barrado y Navascués

[13] http://www.cida.gob.ve/~hernandj/SPTclass/sptclass.html

[14] SIMBAD, Centre de Donneés astronomiques de Strasbourg, at http://simbad.u-strasbg.fr/simbad/.

[15] In general, the spectroscopic features in which we obtain EW show Gaussian profiles.

Table 4
Low Resolution Analysis

Name H07	2massID	INST	Spectral Types	Li I (Å)	Li I Flag	Hα (Å)	Hα Flag	Na I (Å)	Na I Flag	Av_{KH95} (mag)	Av_{PM13} (mag)
...	05384476-0236001	F	B0.0 ± 1.5	0.0	0	3.1	E_{abs}	...	...	0.00	0.00
...	05384561-0235588	F	B2.0 ± 1.5	0.0	0	4.3	E_{abs}	...	...	0.10	0.00
...	05402018-0226082	F	B4.0 ± 1.5	0.0	0	5.0	E_{abs}	...	...	0.17	0.00
SO139	05374047-0226367	F	A3.5 ± 2.5	0.0	0	11.0	E_{abs}	...	...	0.00	0.14
SO521	05382752-0243325	F	A8.0 ± 2.5	0.0	0	8.3	E_{abs}	...	...	0.18	0.84
SO338	05380649-0228494	S	F3.5 ± 2.0	0.1	1	3.5	E_{abs}	...	...	0.72	0.72
SO1352	05400696-0228300	F	F7.5 ± 2.0	0.0	0	3.6	E_{abs}	...	...	1.36	1.44
SO1246	05395118-0222461	H	G1.0 ± 2.5	0.0	0	1.5	E_{abs}	...	...	2.41	2.49
SO550	05383008-0221198	H	G1.5 ± 2.5	0.0	0	1.8	E_{abs}	...	...	2.05	2.12
SO1286	05395658-0246236	H	G5.0 ± 2.5	0.0	0	2.1	nAcr	...	...	1.83	1.70
SO29	05372330-0229133	H	G9.5 ± 2.0	0.0	0	1.8	nAcr	...	...	0.51	0.27
SO449	05381879-0217138	H	K0.0 ± 3.0	0.0	0	0.0	nAcr	...	...	1.00	0.83
SO903	05390828-0249462	F	K5.5 ± 1.5	0.0	0	0.4	nAcr	...	...	0.00	0.00
SO1113	05393511-0247299	F	K5.5 ± 1.5	0.5	2	−1.1	nAcr	...	...	0.41	0.00
SO1274	05395465-0246341	S	K6.0 ± 1.0	0.3	2	−36.5	Acr	...	...	1.40	0.92
SO611	05383546-0231516	H	K7.0 ± 1.0	0.6	2	−2.7	Acr?	...	...	0.48	0.11
SO35	05372384-0248532	H[a]	M0.0 ± 1.5	0.0	1	2.4	nAcr	...	...	0.77	0.46
SO726	05384746-0235252	H	M0.5 ± 1.0	0.4	2	−23.0	Acr	0.94 ± 0.08	...	0.03	0.00
SO682[b]	05384227-0237147	C	M0.5 ± 1.0	0.2	1	−2.7	nAcr	...	...	0.67	0.34
SO600	05383479-0239300	F	M1.0 ± 0.5	0.0	0	0.9	nAcr	...	...	0.71	0.34
SO1282	05395594-0220366	H	M2.0 ± 0.5	0.4	2	−8.2	nAcr	1.37 ± 0.10	...	0.62	0.23
SO444	05381824-0248143	H	M3.0 ± 0.5	0.5	2	−3.8	nAcr	0.83 ± 0.08	Y	0.12	0.08
SO562	05383141-0236338	H	M3.5 ± 1.5	0.1	2	−77.7	Acr	0.52 ± 0.10	Y	0.07	0.14
SO1053	05392650-0252152	H	M4.0 ± 0.5	0.4	2	−3.6	nAcr	1.02 ± 0.09	Y	0.00	0.00
SO300	05380107-0245379	H	M4.5 ± 0.5	0.4	2	−92.6	Acr	0.65 ± 0.10	Y	0.14	0.26
SO460	05382021-0238016	H	M5.0 ± 0.5	0.4	2	−10.6	nAcr	1.44 ± 0.14	Y	0.00	0.00
SO283	05375840-0241262	H	M5.5 ± 0.5	0.6	1	−14.3	Acr?	0.99 ± 0.13	Y	0.00	0.00
SO457	05381975-0236391	F	M6.0 ± 0.5	0.0	0	0.2	nAcr	...	...	0.00	0.32
SO209	05375110-0226074	H[a]	M6.5 ± 2.5	0.0	1	−13.3	nAcr	...	...	...	...

Notes.
INST: see Table 3. Li I flag: (2) Li I is present in absorption; (1) Li I uncertain; (0) Li I is not present on the spectrum. Hα flag: (Acr) accretor; (nAcr) non-accretor; (Acr?) uncertain; (E_{abs}) star earlier than G5 with Hα in absorption; (ET_{em}) star earlier than G5 with Hα in emission. NaI I flag: (Y) member; (N) non-member.
[a] Low signal-to-noise ($S/N \lesssim 15$).
[b] Slow accretor candidate.
[c] Diskless stars that mimic the Hα width expected in stars with accretion disks.

(This table is available in its entirety in a machine-readable form in the online journal. A portion is shown here for guidance regarding its form and content.)

et al. 2003). Using different symbols we plot results obtained using different spectrographs (see Table 3). We also plot stars bearing protoplanetary disks (H07b). In general, stars above the Barrado's accretion cutoff were classified as stars bearing full disks (II) or transitional disks (TD) in H07b. There are some stars with optically thick disks below the Hα EW criterion (SO 435, SO 467, SO 566, SO 598, SO 682, SO 823, and SO 967). These stars would be similar to CVSO 224, which was classified as a weak-line T Tauri star based on the EW of Hα. However, using high-resolution spectra, Espaillat et al. (2008) show that is a slowly accreting T Tauri star with accretion rate of $7 \times 10^{-11}\ M_{\odot}\ \mathrm{yr}^{-1}$ estimated using the magnetospheric accretion models (Muzerolle et al. 2001). On the other hand, there are diskless stars that were classified as accretors (SO 229, SO 1123, and SO 1368). These diskless objects with Hα in emission could have substantial contribution produced by strong chromospheric activity which is related to fast rotation. In Section 4.2, we study in more detail slowly accreting stars and diskless stars that mimic the Hα width expected in stars with accretion disks.

For very low-mass stars (VLMS) observed with HECTOSPEC, we can use the line Na I λ8195 as an additional indicator of youth (Downes et al. 2008). Since VLMS in the σ Orionis cluster are still contracting, their surface gravities are lower than that expected for a main-sequence star with similar spectral type. The line Na I λ8195 is the strongest one of the sodium doublet (Na I λλ8183, 8195), which is sensitive to surface gravity and varies significantly between M-type field dwarf and PMS objects (Schlieder et al. 2012). The EW of the line Na I λ8195 was estimated fitting a Gaussian function to the feature on the normalized spectrum. We use the continuum bands suggested by Schlieder et al. (2012) to normalize each spectrum. The uncertainties in EWs were calculated as in Kenyon et al. (2005) using the scale of HECTOSPEC (∼1.2 Å pixel^{-1}) and the S/N of the continuum bands. Figure 4 shows normalized spectra of three stars with spectral type M5 illustrating the procedure to measure the line Na I λ8195. The sources 05400029+0142097 and 05373723+0140149 are CVSO's stars spectroscopically confirmed as a dwarf field star and as a ∼10 Myr old star, respectively (C. Briceno et al., in preparation). The star SO 460 has Li I λ6708 in absorption and has been confirmed previously as member of the σ Orionis cluster using RV (Zapatero Osorio et al. 2002; Sacco et al. 2008; Maxted et al. 2008). It is apparent that the M-type field star exhibits stronger absorption in the sodium doublet in comparison to the PMS stars.

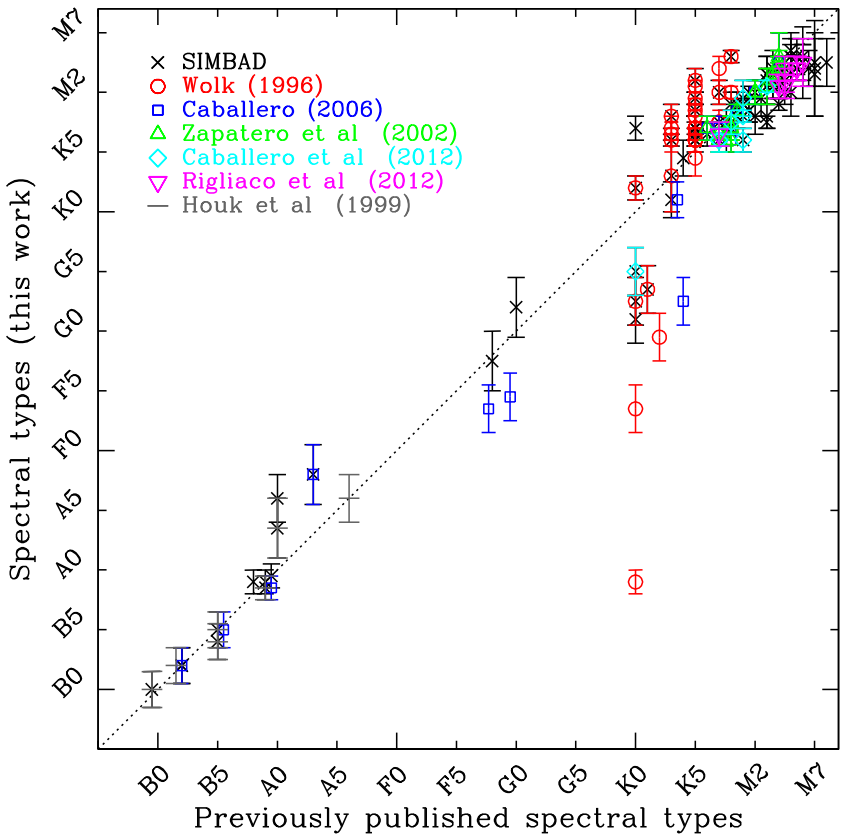

Figure 2. Comparison of spectral types determined in this work with previously published values: Wolk (1996), Caballero (2006), Zapatero Osorio et al. (2002), Caballero et al. (2012), Rigliaco et al. (2012), Houk & Swift (1999), and the SIMBAD database (see references in the text). Vertical error bars are the uncertainties derived from our spectral type classification. For comparison, we show the line with slope 1. For most stars, the spectral types derived in this work agree, within the uncertainties, with previous determinations of spectral types.

(A color version of this figure is available in the online journal.)

Figure 5 shows the EW of Na I λ8195 versus spectral type for stars in the σ Orionis sample, illustrating the procedure of using the sodium line as an additional criteria supporting membership in the VLMS of σ Ori. We display the median and the second and third quartiles of Na I λ8195 measured for a sample of PMS stars (lower solid line) and for a sample of M-type field dwarfs (upper solid line) in the Orion OB1a and OB1b associations (C. Briceno et al., in preparation). These PMS stars, with ages ranging from ∼5 to ∼10 Myr, were confirmed by the presence of Li I λ6708 in absorption. In general, stars confirmed as members by the presence of Li I λ6708 in the σ Orionis cluster (open squares) are below the median population of PMS stars in the OB1a and OB1b associations. On the other hand, stars selected as non-members of the σ Orionis cluster (open circles) follow the median line of M-type field dwarfs in the OB1a and OB1b associations. Figure 5 shows that the separation between M-type field stars and PMS stars is more clear for later spectral types, so that for stars with spectral type M3 or later we use the EW of Na I λ8195 as an additional criteria of youth; those stars located below the median line of the PMS stars in the OB1a and OB1b associations were identified as young stars (labeled with "Y" in Column 10 of Table 4). Most of the σ Ori VLMS with uncertain membership based on Li I λ6708 (crosses) have smaller values of EW of Na I λ8195 and thus are likely members of the cluster. The stars SO 576 and SO 795 exhibit strong Na I λ8195 line and thus are classified as M-type field stars (labeled with "N" in Table 4)

In order to estimate reddening for our sample, we calculate the rms of the differences between the observed colors and the standard colors

$$\mathrm{rms}(A_V) = \sqrt{\frac{\sum([V-M_\lambda]_{\mathrm{obs}} - \left[1-\frac{A_\lambda}{A_V}\right] * A_V - [V-M_\lambda]_{\mathrm{std}})^2}{n}}, \quad (1)$$

where $[V-M_\lambda]_{\mathrm{obs}}$ are the observed colors V-Rc, V-Ic, and $V-J$ (when they are available), n is the number of colors used to calculate rms(A_V), and $[V-M_\lambda]_{\mathrm{std}}$ are the corresponding standard colors for a given spectral type. The values of A_λ/A_V were obtained from Cardelli et al. (1989) assuming the extinction law normally used for interstellar dust ($A_\lambda/A_V = 0.832$, 0.616 and 0.288 for Rc, Ic, and J, respectively). We vary the visual extinction (A_V) from 0 to 10 mag in steps of 0.01 mag and estimate visual extinction as the A_V value with the lowest rms(A_V). We use the intrinsic colors for main-sequence stars from Kenyon & Hartmann (1995) and the intrinsic colors of 5–30 Myr old PMS stars from Pecaut & Mamajek (2013). Since these PMS intrinsic colors are given for stars F0 or later, we complete the standard colors for stars earlier than F0 using the intrinsic color of 09–M9 dwarf stars compiled by Pecaut & Mamajek (2013). Intrinsic colors of PMS stars earlier than G5 appear to be consistent with the dwarf sequence (Pecaut & Mamajek 2013).

Since PMS stars are in a different evolutionary stage than dwarf field stars, there may be systematic errors in the calculation of interstellar reddening when using main-sequence calibrators. Figure 6 shows a comparison between the reddening calculated using the intrinsic colors for main-sequence stars from Kenyon & Hartmann (1995) and the intrinsic colors for PMS stars from Pecaut & Mamajek (2013). In

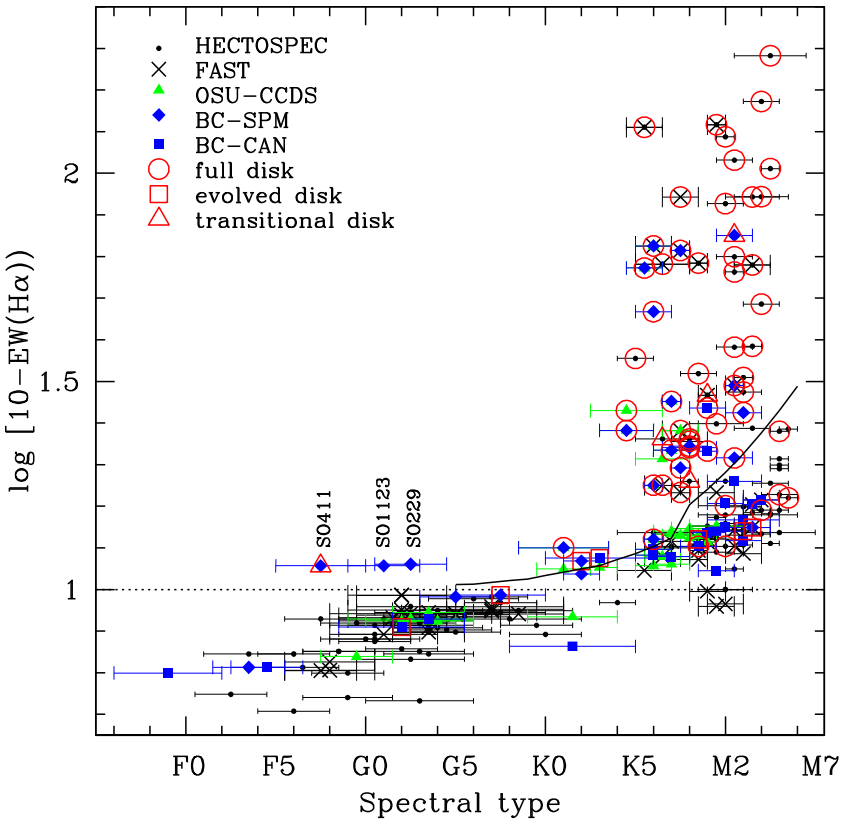

Figure 3. Relation between the EW of Hα and the spectral type. In order to plot our data in a logarithmic scale, EWs have been shifted by 10 units. Solid line indicates the limit for classical and weak-line T Tauri stars based on the H_α in emission (Barrado y Navascués et al. 2003). Dotted line indicates the limit between emission and absorption of H_α. We plot, with different symbols, spectra obtained from different spectrographs (see Table 3). We also indicate the disk type for the sample using *Spitzer* photometry (H07b).

(A color version of this figure is available in the online journal.)

general, for stars in the spectral type range from G2 to M3, the visual extinctions estimated from Kenyon & Hartmann (1995), are larger than those estimated using PMS colors (Pecaut & Mamajek 2013). On the other hand, for stars later than M3 (open squares), visual extinctions estimated from Kenyon & Hartmann (1995), are slightly smaller than those estimated using PMS colors (Pecaut & Mamajek 2013).

Sorted by spectral types, Table 4 summarizes the results obtained from the low-resolution data set. Column 3 indicates the spectrograph used for each star (see Table 3). Column 4 shows spectral types. Columns 5, 7, and 9 show the EWs of Li I λ6708, H_α, and Na I λ8195, respectively. Flags based on these lines are shown in Columns 6, 8, and 10. Columns 11 and 12 show visual extinctions calculated using standard colors for main-sequence stars (Kenyon & Hartmann 1995) and using standard colors for PMS stars (Pecaut & Mamajek 2013).

3.2. Radial Velocity, H_α, and Li I λ6708 Measurements

We measured heliocentric RVs in the high-resolution spectra of the sample observed with Hectochelle. RVs were derived using the IRAF package "rvsao" that cross-correlate each observed spectrum with a set of templates of known RVs (Tonry & Davis 1979; Mink & Kurtz 1998). We used the synthetic stellar templates from Coelho et al. (2005) with solar metallicity, surface gravity of log(g) = 3.5 and effective temperature ranging from 3500 to 7000 K in steps of 250 K. The use of synthetic templates enables us to explore a wider range of stellar parameters than a few observed templates (Tobin et al. 2009). We estimated the RV and the template as those that gave the highest value of the parameter R, defined as the S/N of the cross correlation between the observed spectrum and the template. The RV error is calculated from the parameter R as (Tobin et al. 2009):

$$\mathrm{RV_{err}} = \frac{14(\mathrm{km\,s^{-1}})}{1+R}. \quad (2)$$

In Table 5, we report RVs for 95 stars in which R is larger than 4 (Rverr $\lesssim 2.8$ km s^{-1}). This sample includes 36 stars with known RVs compiled in Section 2.3. In general, the differences between our measurements and known RVs were less than 2 km s^{-1} (rms = 1.9 km s^{-1}). There are five stars (SO 616, SO 662, SO 791, SO 929, and SO 1094) with differences larger than 2 km s^{-1}. Since during its orbit around the center of mass RVs of the components of binaries could change, these five stars are labeled as binary candidates by radial velocity variability (RVvar). The cross-correlation function also can be used to identify double-lined spectroscopic binaries (SB2). We have identified four SB2 stars that show double peaks in the cross-correlation function.

EWs of the Li I λ6708 line reported in Table 5 were calculated fitting a Gaussian function to the line in the high-resolution spectra. The errors of EWs were calculated as in Kenyon et al. (2005) using the scale of HECTOCHELLE (0.″0786 pixel^{-1}) and the S/N of the continuum used to obtain the EW. Figure 7 shows a diagram of EWs of Li I λ6708 versus RVs. The distribution of RVs can be described by a Gaussian function centered at 30.8 km s^{-1} with a standard deviation (σ_{RV}) of 1.7 km s^{-1}. Applying a $3\sigma_{\mathrm{RV}}$ criteria, we can define a RV range for kinematic

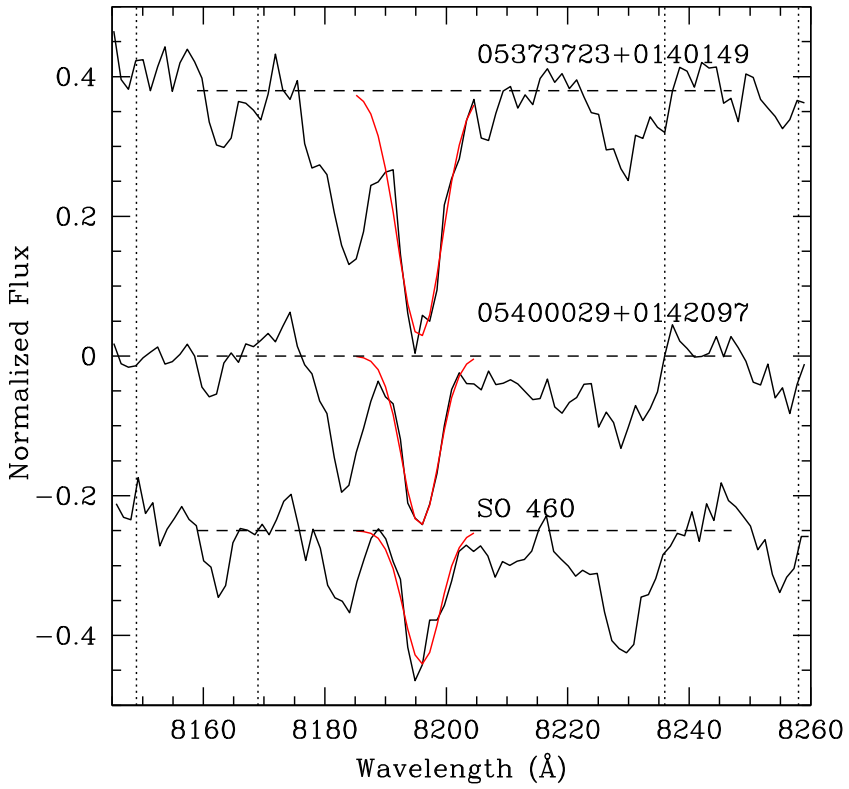

Figure 4. Normalized spectra of the sodium doublet (Na I λλ8183, 8195) for three M5-type stars at different evolutionary stages. Vertical dotted lines represent the limits of the continuum bands used to normalize the spectra (Schlieder et al. 2012). A Gaussian function (blue line) was used to calculate the EW of the line Na I λ8195. The M-type field dwarf (upper spectrum) exhibits the strongest absorption of this feature. The PMS star (middle spectrum) located in the 25 Ori stellar cluster (age ∼ 10 Myr; Briceño et al. 2007) exhibits fainter Na I λ8195 than the M-type field dwarf, but stronger absorption than the stars in the σ Orionis cluster (lower spectrum). (A color version of this figure is available in the online journal.)

Table 5
High-resolution Analysis

Name H07	2massID	RV (km s^{-1})	RV Flag	Li I (Å)	W10_Hα (km s^{-1})	Accretor	Disk Type	Comments
SO52	05372692-0221541	9.6 ± 0.3	0	···	···	···	III	Hα in absorption, SB2
SO59	05372806-0236065	29.8 ± 0.9	2	···	115.203	N	III	
SO74	05373105-0231436	···	···	···	···	···	III	Hα in absorption with central emission
SO247	05375486-0241092	···	···	0.25 ± 0.12	192.322	N	II	
SO300	05380107-0245379	···	···	···	413.678	Y	II	
SO341	05380674-0230227	33.7 ± 0.6	2	0.59 ± 0.07	427.684	Y	II	
SO374	05380994-0251377	30.0 ± 0.6	2	0.44 ± 0.06	411.430	Y	II	
SO411	05381412-0215597	22.2 ± 1.1	1	0.16 ± 0.01	294.276	Y	TD	
SO489	05382354-0241317	···	···	0.41 ± 0.17	143.305	N	III	
SO514	05382684-0238460	···	···	···	···	···	II	Inverse P Cygni profile
SO518	05382725-0245096	28.8 ± 0.6	2	0.43 ± 0.02	575.190	Y	II	
SO539	05382911-0236026	33.2 ± 0.7	2	0.77 ± 0.10	152.280	N	III	
SO548	05382995-0215405	···	···	···	133.636	N	III	
SO616	05383587-0230433	23.8 ± 5.6	1	0.82 ± 0.03	465.422	Y	III	RV_{VAR}
SO697	05384423-0240197	29.4 ± 0.2	2	0.56 ± 0.02	198.812	N	II	
SO752	05384945-0249568	−49.2 ± 0.6	0	···	···	···	III	Double central absorption
SO1097	05393291-0247492	27.8 ± 1.3	2	0.59 ± 0.03	168.462	N	III	
SO1251	05395253-0243223	46.0 ± 0.2	0	0.08 ± 0.04	···	···	III	Hα in absorption, EW[Li I] < 0.1
SO1352	05400696-0228300	34.9 ± 0.2	2	···	···	···	III	Hα in absorption
SO1361	05400889-0233336	30.1 ± 0.6	2	0.48 ± 0.02	362.225	Y	II	
SO1370	05401304-0228314	···	···	···	···	···	III	Hα in absorption

Notes.
RV flag: (2) kinematic member; (1) sparser stellar population candidate; (0) kinematic non-member. Accretor flag: (Y) accretor (W10_Hα > 270 km/s); (N) non-accretor (W10_Hα < 270 km s^{-1}). Disk type: III = diskless, II = thick disk, I = class I, EV = evolved disk, TD = transition disk, DD = Debris disk. RV_{var}: binary candidate by radial velocity variability. SB2: binary candidate identified in the cross correlation function.

(This table is available in its entirety in a machine-readable form in the online journal. A portion is shown here for guidance regarding its form and content.)

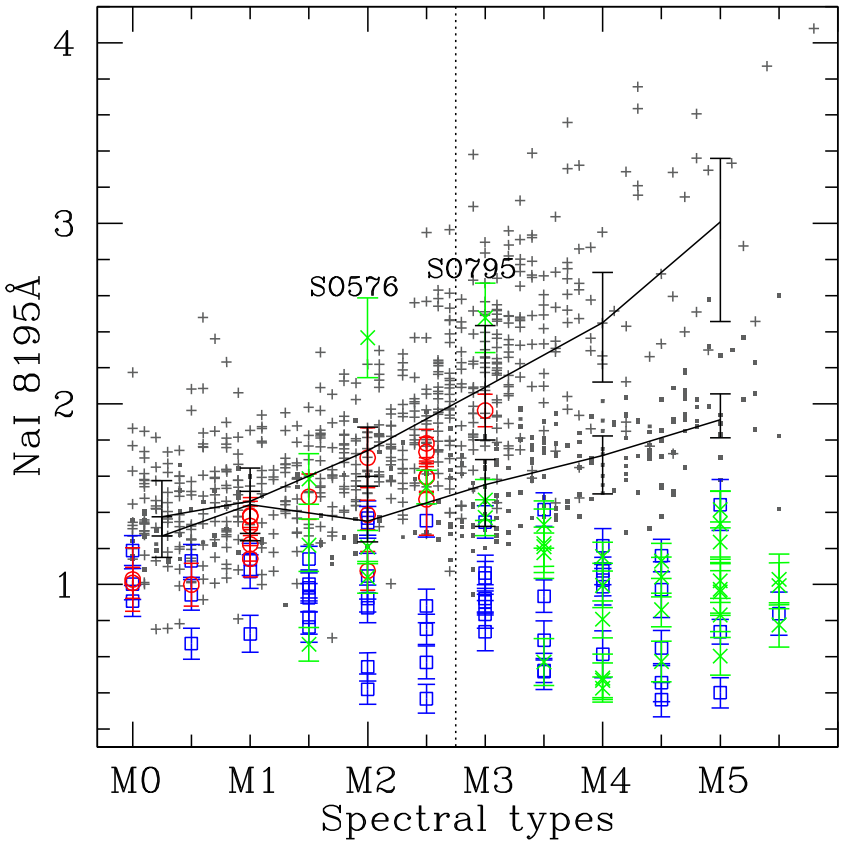

Figure 5. Relation between the EW of Na I λ8195 and the spectral type for the sample of stars observed with Hectospec. We display the median and the second and third quartiles of Na I λ8195 measured for a sample of PMS stars (age range ∼5–10 Myr; dots and lower solid line) and for a sample of M-type field dwarfs (plus symbol and upper solid line) in the Orion OB1 association (C. Briceno et al., in preparation). Open squares and open circles indicate stars in the σ Orionis cluster with and without Li I λ6708, respectively. In general, stars with uncertain membership based on Li I λ6708 (crosses) have smaller values of EW of Na I λ8195. Using the sodium criteria, we identify as member of the σ Orionis cluster stars with spectral type M3 or later and located below the median values of the PMS population in the Orion OB1 association. The stars SO 576 and SO 795 were identified as M-type field stars.

(A color version of this figure is available in the online journal.)

members of the cluster from 25.7 km s^{-1} to 35.9 km s^{-1}. These values are similar to those reported by Jeffries et al. (2006) for the stellar group associated with the star σ OriAB (27–35 km s^{-1}). In Table 5, we label as kinematic members of the σ Orionis cluster stars with RV in the membership range (flag "2") and as kinematic candidates of the sparser stellar population (see Section 2.3) stars with RVs from 20 km s^{-1} to 25.7 km s^{-1} (flag "1"). Stars with RV smaller than 20 km s^{-1} and larger than 35.9 km s^{-1} were flagged as kinematic non-member (flag "0"). Three stars with Li I λ6708 in absorption fall in the last group. The stars SO 362 and SO 1251 have RV $>$ 35.9 km s^{-1} and the star SO 243 has RV $<$ 20 km s^{-1}. The star SO 362 has a protoplanetary disk and its discrepant RV value could be caused by binarity. The Li I λ6708 measured in the star SO 1251 is lower than those expected for the σ Orionis stellar population and thus its membership is uncertain. Since the spectral type of the star SO 243 is relatively early (G5; see Section 3.1), the youth of this object is also uncertain. The shallow depth of the convective zone in stars earlier than K0 can allow them to reach the main sequence with a non-negligible amount of their primordial lithium content and thus Li I λ6708 in absorption is not a reliable indicator of the PMS nature of these stars. Therefore, the presence of lithium in absorption in F-type and G-type stars is only evidence that these objects are not old disk, post-main-sequence stars (Briceno et al. 1997). Finally, we were unable to calculate RVs for 17 stars with Li I λ6708 in absorption. These stars were included as spectroscopic members of the cluster.

The full width of H$_\alpha$ at 10% of the line peak (WH$_\alpha$_10%) is an indicator that allows to distinguish between accreting and non-accreting young stellar objects. White & Basri (2003) suggested that WH$_\alpha$_10% $>$ 270 km s^{-1} indicates accretion independent of the spectral type. Jayawardhana et al. (2003) adopted a less conservative accretion cutoff of 200 km s^{-1} studying young very low-mass stars and brown dwarfs. A newly born star is surrounded by a primordial optically thick disk that evolves due to viscous processes by which the disk is accreting material onto the star while expanding to conserve angular momentum (Hartmann et al. 1998). As a consequence of this and other evolutionary processes, the frequency of accretors and the accretion rate in the inner disks steadily decreases from 1 to 10 Myr (e.g., Calvet et al. 2005; Williams & Cieza 2011). Thus signatures of accretion can be used as indicators of membership in a young stellar region. In the case in which Hα has a symmetric or quasi-symmetric profile in emission, we measured automatically the peak of the profile fitting a Gaussian function to the Hα line. When the fitting of a single Gaussian function does not work (e.g., non-symmetric profiles), the peak of the Hα line was selected manually. The WH$_\alpha$_10% was measured as the width of the Hα velocity profiles at 10% of the emission peak level (Column 6 in Table 5). Following the criterion from White & Basri (2003), stars with WH$_\alpha$_10% $>$ 270 km s^{-1}

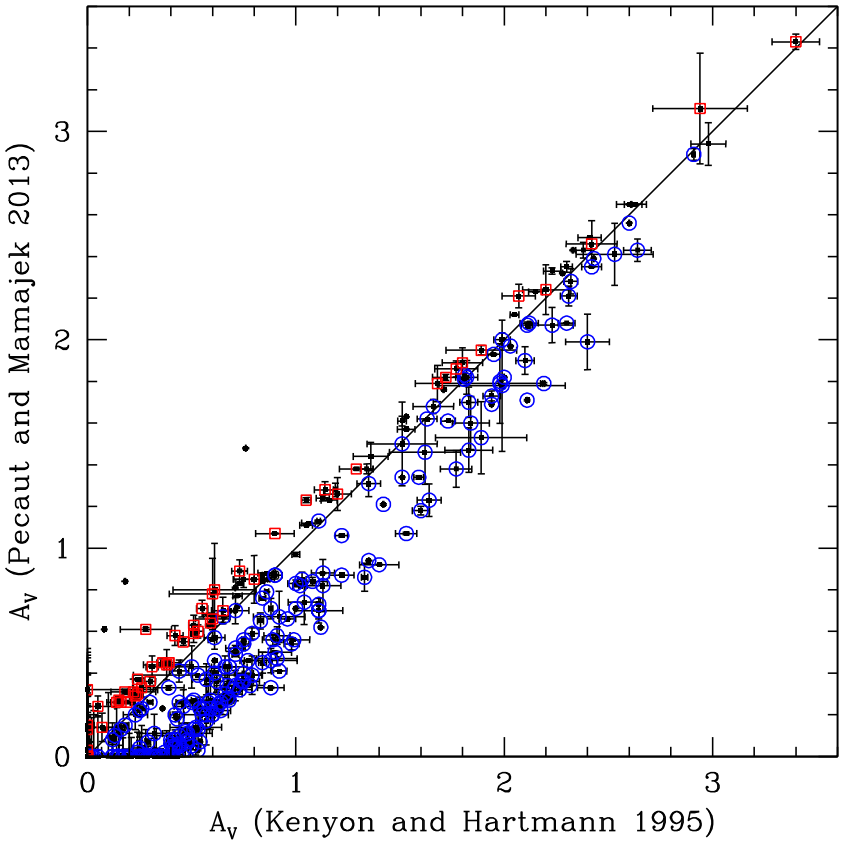

Figure 6. Comparison between interstellar reddening calculated using the intrinsic colors for main-sequence stars (Kenyon & Hartmann 1995) and the intrinsic colors for PMS stars (Pecaut & Mamajek 2013). Open squares indicate stars with spectral types later than M3 and open circles indicate stars with spectral types ranging from G2 to M3.

(A color version of this figure is available in the online journal.)

were identified as accretors. Stars without measurements of WH_{α}_10% have comments in Table 5 about the Hα profile.

3.3. Additional Criteria for Membership

Since the criteria used in Section 3.1 as indicators of youth are useful mainly for stars with spectral types K and M, we need to use additional criteria to confirm or reject candidates as member of the σ Orionis cluster. In general, the memberships described in this section are less reliable than those obtained from low-resolution spectroscopic analysis (Section 3.1) and those obtained from high-resolution spectroscopic analysis (Section 3.2).

3.3.1. Photometric Membership Probabilities and Variability

PMS stars are characterized by having a high degree of photometric variability of diverse nature (Herbst et al. 1994; Cody & Hillenbrand 2010, 2011). The variability is due to chromospheric and magnetic activity in the stellar surface (e.g., cool spots, flares, and coronal mass ejections) and to protoplanetary disks around the stars (e.g., hot spots produced by accretion shocks, variable accretion rates, and variable extinction produced by inhomogeneities in the dusty disk). Since the expected photometric variability in PMS stars are so diverse, it is difficult to apply variability criteria such as range of periods or light curve types to refine the selection of possible members of a young stellar group. However, we can use the location of variable stars in color–magnitude diagrams to select them as PMS candidates. Briceño et al. (2001, 2005) indicate that selecting variable stars above the ZAMS located at the typical distance of a young stellar group clearly picks a significant fraction of members of that stellar group. Moreover, using the differences between the observed colors and the expected colors defined by empirical or theoretical isochrones, we can calculate photometric membership probabilities for the sample.

Figure 8 shows the procedure to estimate photometric membership probabilities. Based on $[V-J]$ colors and V magnitudes, we tailored new indices ($C_{\rm rot}$ and $M_{\rm rot}$) using the following equations to rotate the color–magnitude diagram of Figure 1:

$$C_{\rm rot} = [V - J] * \cos(\theta) - (V - V_0) * \sin(\theta) \quad (3)$$

$$M_{\rm rot} = V_0 + [V - J] * \sin(\theta) + (V - V_0) * \cos(\theta), \quad (4)$$

where V_0 is the V value where the empirical isochrone has $[V-J] = 0$ and θ is the angle where the rms of $C_{\rm rot}$ for the known member sample is minimal ($\sim 25\overset{\circ}{.}5$). The distribution of $C_{\rm rot}$ for known members (open circles) describes a Gaussian function with standard deviation of $\sigma = 0.32$. Assuming a standard normal distribution we can transform $C_{\rm rot}$ values to probabilities for our sample. The 3σ criterion applied in Section 2.5.5 to select photometric candidates means that stars that fall outside of this criteria have membership probabilities lower than ~0.3% (dotted lines in Figure 8). Notice that the photometric probability obtained here does not take into account the distribution of non-members in Figure 8. The contamination by non-members is much higher at negative values of $C_{\rm rot}$ than at positive values

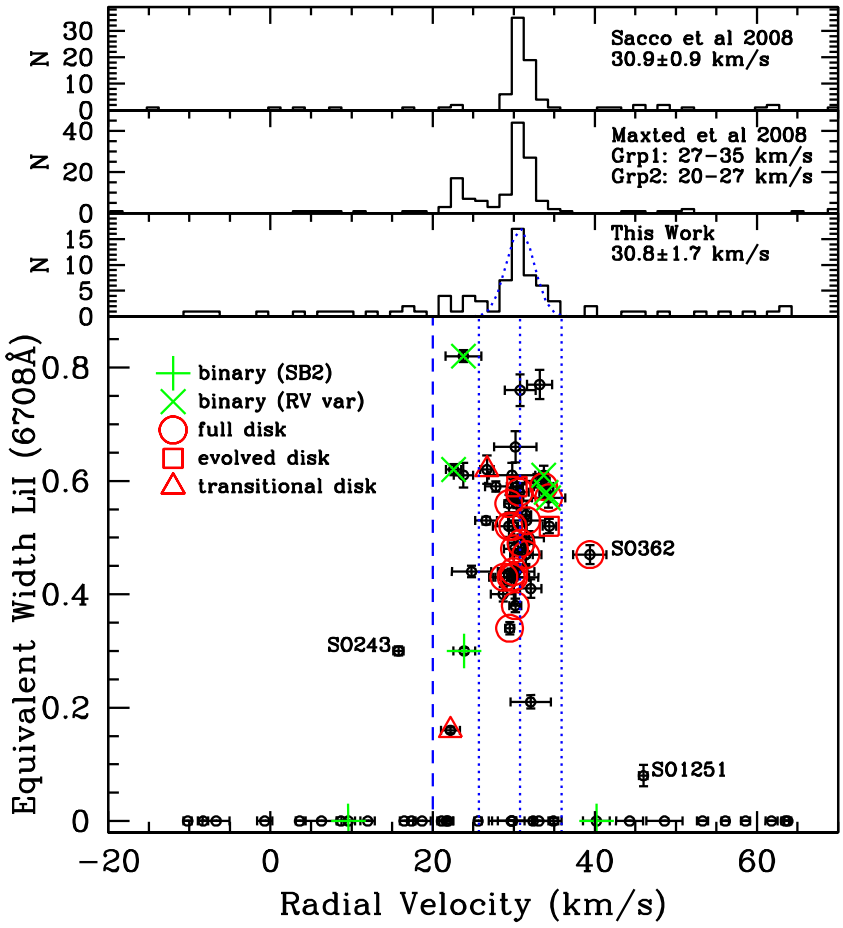

Figure 7. Equivalent width of Li I λ6708 vs. RV obtained from Hectochelle data. Our RV distribution (third panel) is in agreement with the RV distribution obtained by Sacco et al. (2008, first panel) and with the RV distribution of group 1 from Maxted et al. (2008, second panel). A Gaussian function was fitted to our RV distribution. The dotted vertical lines represent the center of the Gaussian and the 3σ criteria used to identify kinematic members of the cluster. The dashed line represents the lower limit for the sparser stellar population (see Section 2.3). Disk types from H07b are plotted. We show binaries exhibiting double peaks in the correlation function (SB2) or binaries identified by radial velocity variability (RV var). Stars with Li I λ6708 in absorption located to the left of the kinematic regions can be candidates of a more sparser and older group (group 2 in Maxted et al. 2008) or binary candidates of the cluster. The stars SO 243, SO 362, and SO 1251 are located in the kinematic non-members region.

(A color version of this figure is available in the online journal.)

of $C_{\rm rot}$. Also, the expected contamination is higher at $M_{\rm rot}$ ∼13 where a branch of old field stars crosses the stellar population of the σ Orionis cluster.

We plot in Figure 8 variable stars reported in the CVSO catalog (Briceño et al. 2005; Mateu et al. 2012), stars flagged as variable in the cluster collaboration's photometric catalogs (Kenyon et al. 2005; Mayne et al. 2007), variable low-mass stars and brown dwarfs of the σ Orionis cluster (Cody & Hillenbrand 2010), and stars listed as known or suspected variables in The AAVSO International Variable Star Index (Watson 2006). In spite of the fact that this compilation of variable stars in the σ Orionis cluster is not complete, 60% of the stars within the 1σ criteria (dotted lines; photometric probability higher than ∼32%) are reported as variable objects.

3.3.2. Proper Motion and Spatial Distribution

In general, the motion of young stellar groups of the Orion OB1 association are mostly directed radially away from the Sun. Thus, the expected intrinsic proper motions in right ascension ($\cos(\delta) * \mu_\alpha$) and declination ($\mu_\delta$) are small and comparable to measurement errors (Brown et al. 1998; Hernández et al. 2005). Particularly, Brown et al. (1998) reported an average proper motion for this stellar association of 0.44 mas yr^{-1} and −0.65 mas yr^{-1} for $\cos(\delta) * \mu_\alpha$ and μ_δ, respectively. Although we cannot use proper motion to separate potential cluster members from field star non-members, we can use criteria based on proper motions to identify and reject high proper motion sources as potential members of the σ Orionis cluster (e.g., Lodieu et al. 2009; Caballero 2010).

We follow a similar method used in Hernández et al. (2009) to identify potential non-members of the cluster. Figure 9 shows the vector point diagram for the photometric candidates with proper motions reported in the fourth US Naval Observatory CCD Astrograph Catalog (UCAC4; Zacharias et al. 2013). The distributions of proper motions for the known members (green X's) can be represented by Gaussians centered at $\cos(\delta) * \mu_\alpha$ ∼ 2.2 mas yr^{-1} and μ_δ ∼0.7 mas yr^{-1}, with standard deviations of 5.3 mas yr^{-1} and 4.1 mas yr^{-1}, respectively. These values agree within the errors with previous estimations for the entire OB association (e.g., Brown et al. 1998) and for the cluster (e.g., Kharchenko et al. 2005; Caballero 2007, 2010). Most known members (∼86%) are located in a well defined region represented for the 3σ criteria (dotted ellipse) in the vector point plot. We also use a less conservative criteria of 5σ (solid line ellipse) similar to the criteria used in previous works (Caballero 2007, 2010; Lodieu et al. 2009). With the exception of the stars

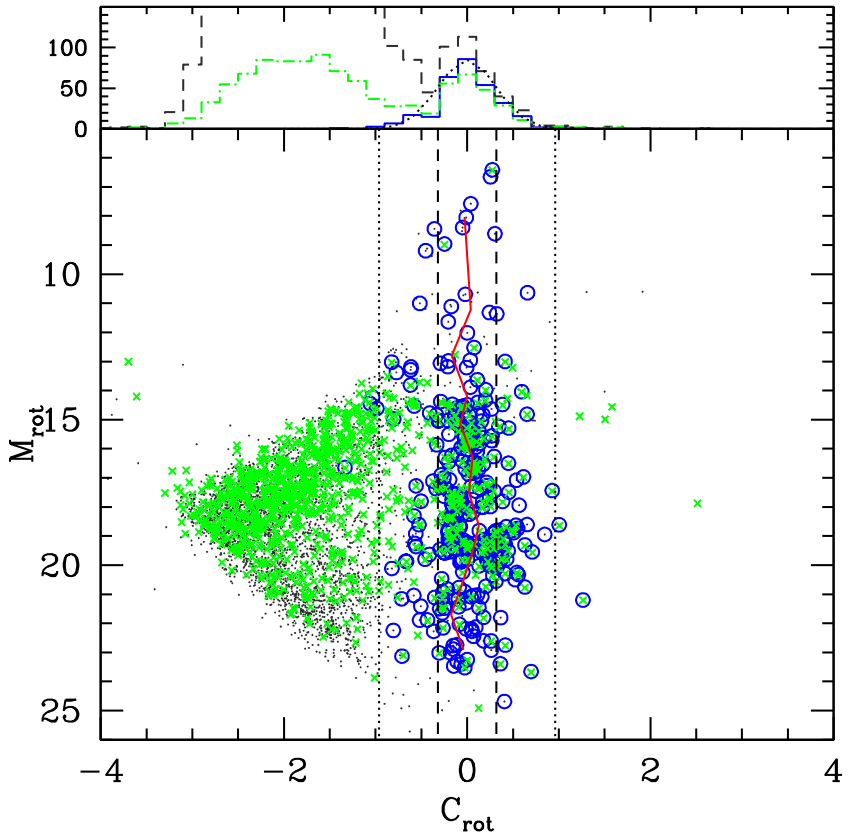

Figure 8. Diagram used to calculate photometric probabilities. The color–magnitude diagram of Figure 1 was rotated in order to get the new variable C_{rot} near zero for the known member sample (open circles and solid histogram in the upper panel). The red solid line represents the empirical isochrone. A Gaussian function (dotted histogram) was fitted to the C_{rot} distribution of the known members. Stars identified as variables are plotted with symbol "X." Stars within the dotted vertical lines have photometric probabilities larger than 0.3% ($|C_{rot}| < 3\sigma$). Stars within the dashed vertical lines have photometric probabilities larger than 31.7% ($|C_{rot}| < 1\sigma$). The dotted-dashed histogram and the long dashed histogram represent the distribution of variable stars and the distribution of the entire sample, respectively.

(A color version of this figure is available in the online journal.)

SO 592, SO 936, and SO 1368, the 5σ criteria includes all the known member sample. The star SO 592 is a RV member with Li I λ6708 in absorption (see Section 2.6). The star SO 1368, reported as diskless accretor in Section 3.1, has large error in $\cos(\delta)*\mu_\alpha \sim$ and thus the proper motion criteria for this object is uncertain. The star SO936 lies outside the vector point diagram. Its infrared excess at 8 μm (H07b) is the only youth feature reported for this photometric candidate. Astrometric followup could help to find out if those stars are members of binary systems, they were ejected from the cluster early on during the formation process or they belong to a moving group associated with Orion (Lodieu et al. 2009).

Based on the distribution of stars in the vector point diagram, we have classified our photometric candidates into three groups, stars inside of the 3σ limit (proper motion flag "2"), stars between the 3σ and the 5σ limit (proper motion flag "1") and stars with proper motions larger than the 5σ criteria (proper motion flag "0"). In general, the proper motion flags agree with previous proper motion studies to identify high proper motion interlopers (Lodieu et al. 2009; Caballero 2010). Out of 29 stars studied by Caballero (2010) and located in the region studied in this work, 14 stars have proper motion in UCAC4. All the 13 photometric candidates identified by Caballero (2010) as high proper motion interlopers have proper motion flag "0." The other star is a background star (Section 2.4) rejected using optical colors (star #38 in Caballero 2010). Only one star (05401975-0229558) reported by Lodieu et al. (2009) as proper motion non-member have proper motion flag "1." Additional studies are necessary to obtain youth features of this object.

Finally, Caballero (2008b) suggests that the σ Orionis cluster has two components: a dense core that extends from the center to a radius of 20′ and a rarefied halo at larger separations. Members of the σ Orionis cluster have higher probability to be located in the dense core than in the rarefied halo. Thus, we also include a flag for the distance from the center of the cluster. Stars located closer than 20′ have flag "1," otherwise they have flag "0."

3.4. Membership Analysis of the Cluster

Depending on the spectral type range, obtaining memberships of stars that belong to a young stellar group can be a difficult process and some times we need to combine different membership indicators. Based on the spectroscopic and photometric analysis developed in Sections 2.4, 4.1, 3.2, 3.1, and 3.3, and the information compiled in Section 2.3 about several membership criteria, we compile in Table 6 membership indicators for stars with spectral types obtained in Section 3.1. Columns 1 and 2 show source designations from H07b and Cutri et al. (2003), respectively. Column 3 shows the spectral type. Column 4 indicates the membership flag based on the presence of Li I λ6708 in absorption from low-resolution spectra (Section 3.1) and from high-resolution spectra (Section 3.2). Column 5 shows the references of known members based on Li I λ6708. Columns 6 and 7 show the RV information from our analysis (Section 3.2) and

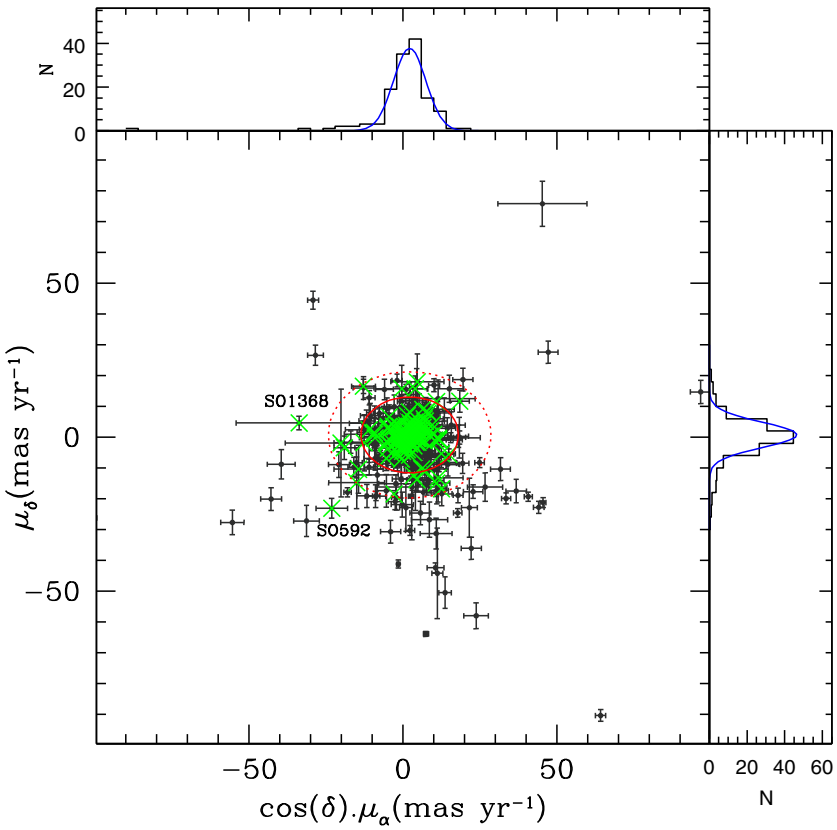

Figure 9. Vector point diagram for photometric candidates. Green crosses indicate the position of the known member sample, and the upper panel and right panel show its proper motion distribution in right ascension and declination, respectively. Gaussian function curve fitting indicates that those distributions are centered at $\cos(\delta) * \mu_\alpha \sim 2.2 \pm 5.3$ mas yr^{-1} and $\mu_\delta \sim 0.7 \pm 4.1$ mas yr^{-1}. About 86% of the known members are located within the 3σ limit (dotted ellipse). Almost all known members are located within 5σ (solid ellipse) from the center of the distributions. Only the known members SO592, SO936, and SO1368 are located beyond the 5σ criteria.

(A color version of this figure is available in the online journal.)

from previous works, respectively. Column 8 shows the classification based on the Hα line and the accretion criteria from Barrado y Navascués et al. (2003, Section 3.1) and from White & Basri (2003, Section 3.2). Column 9 indicates the membership flag based on the line Na I λ8195 (Section 3.1). Additional membership information based on the presence of protoplanetary disks, X-ray emission, proper motion, distance from the center of the cluster, and variability are in Columns 10, 11, 12, 13, and 14, respectively. Column 15 gives the photometric membership probability calculated in Section 3.3 and Column 16 indicates the visual extinction estimated using the PMS standard colors of Pecaut & Mamajek (2013, Section 3.1). Finally, our membership flags and comments are given in the last column. Similar to the membership study by Kenyon et al. (2005), some of our membership flags are arguable, but the reader can reach their own conclusions based on the information in Table 6.

In general, stars with spectral types B or A in Table 6 were included as young stars by Caballero (2007) and Sherry et al. (2008) using proper motion, RV, X-ray, and infrared observations and main sequence fitting analysis. The star SO 602 was not included in those studies. This star has discrepant RV and very high visual extinction to be considered member of the σ Orionis cluster. The star SO 147 was not included in Sherry et al. (2008) and was rejected by Caballero (2007) based on the proper motions reported by Perryman et al. (1997). SO 147 is a X-ray source and our RV measurements indicate that could be a young star member of the sparser population (Maxted et al. 2008) or a binary of the σ Orionis cluster. However, the visual extinction of SO 147 is higher than that expected for the cluster, thus its membership is uncertain. Sherry et al. (2008) suggested that SO 956 is too bright to be a member of the cluster and SO 521 is too faint to be a member of the cluster. The star SO 956 has youth features like infrared excess and X-ray emission and the star SO 521 is located above the ZAMS but with relatively low photometric membership probability. Thus is not clear the membership status of these two objects. Finally, the star SO 139 is relatively bright to be a member of the cluster and Sherry et al. (2008) suggested that it could be a member of the cluster if this star is an equal mass binary. In summary, the memberships of the stars SO 139, SO 956, SO 521, and SO 147 reported in Table 6 are uncertain.

It is more difficult to estimate membership for solar-type stars (F and G). In this spectral type range, old stars cross the sequence defined by the σ Orionis cluster and thus the contamination level by non-members of the cluster is quite high. For some stars, Li I λ6708 appears in absorption. However, for solar-type stars, this is not a robust criteria of youth and it is only evidence that these objects are not old disk, post-main-sequence stars (Briceno et al. 1997; Hernández et al. 2004). Thus, we need to evaluate other membership indicators like presence of disks, X-ray emission, variability, RV proper motions, reddening, and photometric membership probabilities to confirm or reject stars as members of the cluster. In Table 6, solar-type stars with Li I λ6708 in absorption have additional youth features that support their membership of the cluster (mainly X-ray source, infrared excesses, and variability). Four stars with Li I λ6708

Table 6
Membership for Stars with Spectral Types

Name H07	2massID	Spectral Types	Li I Flag Low	Li I Flag High	Li I Ref.	RV Flag	RV Ref.	Hα Flag Low	Hα Flag High	NaI Flag	Disk Type	X-Ray Ref.	PM Flag	Dist Flag	Var Ref.	$\%_{pho}$	A_V	Member Flag
···	05384476-0236001	B0.0 ± 1.5	0	···	···	···	···	E_{abs}	···	···	···	14,15,17,18,19	2	1	···	0.1	0.00	M:[a]
SO139	05374047-0226367	A3.5 ± 2.5	0	···	···	···	···	E_{abs}	···	···	···	···	2	1	···	86.1	0.14	U:[c]
SO411	05381412-0215597	F7.5 ± 2.5	2	2	···	1	···	E_{em}	Y	···	TD	14	2	0	···	95.1	0.07	M:
SO37	05372414-0225520	G0.5 ± 2.0	0	···	···	···	···	E_{abs}	···	···	···	···	2	0	···	···	···	U:
SO1307	05395930-0222543	G2.0 ± 2.5	2	···	···	···	···	E_{abs}	···	···	III	14	2	0	···	44.9	0.63	P:
SO981	05391807-0229284	G7.5 ± 2.5	1	···	···	···	···	nAcr	···	···	DD	14,17,18,19	2	1	···	52.4	0.56	M:
···	05392639-0215034	K4.5 ± 2.0	2	···	6	···	···	Acr	···	···	II	···	2	0	21,22,24	32.7	0.36	M:[19]
SO670	05384135-0236444	M2.0 ± 1.0	1	···	8	···	8,13	···	···	···	III	15,18,19	···	1	···	42.3	0.30	M:
SO27	05372306-0232465	M3.0 ± 1.0	1	···	···	···	···	nAcr	···	Y	III	19	···	0	···	7.4	0.57	P:
SO545	05382961-0225141	M4.0 ± 1.5	1	···	5,12	···	···,5	···	···	···	III	···	···	1	24	79.3	2.21	M:
SO466	05382089-0251280	M5.5 ± 2.0	1	···	···	···	13	Acr?	···	···	III	···	···	1	···	87.1	0.61	M:
SO457	05381975-0236391	M6.0 ± 0.5	0	0	···	···	···	nAcr	Y	···	I	···	2	1	22	0.0	0.32	N:[22]
SO209	05375110-0226074	M6.5 ± 2.5	1	···	···	···	···	nAcr	···	···	III	···	···	1	···	···	···	U:

Notes.
Disk type: III = diskless, II = thick disk, I = class I, EV = evolved disk, TD = transition disk, DD = Debris disk. Member-flag: M: member, N: non-member, U: uncertain, P: probable member, U: uncertain member.
[a] σ Orionis AB: multiple system.
[b] HD37699: probable disk detected using IRAS (Caballero 2007).
[c] HD37333: it is a member if is a equal mass binary (Sherry et al. 2008).
[d] HD37564: it is too bright to be a cluster member (Sherry et al. 2008).
[e] HD294273: it is too faint to be a cluster member (field star; Sherry et al. 2008).
References. (1) Wolk 1996; (2) Zapatero Osorio et al. 2002; (3) Barrado y Navascués et al. 2003; (4) Andrews et al. 2004; (5) Kenyon et al. 2005; (6) Caballero 2006; (7) González Hernández et al. 2008; (8) Sacco et al. 2008; (9) Caballero et al. 2012; (10) Alcalá et al. 1996; (11) Caballero et al. 2006; (12) Muzerolle et al. 2003; (13) Maxted et al. 2008; (14) Caballero 2008a; (15) Skinner et al. 2008; (16) López-Santiago & Caballero 2008; (17) Caballero et al. 2009; (18) Caballero 2010; (19) XMM-SSC, 2010); (20) Burningham et al. 2005; (21) CVSO (Briceño et al. 2005); (22) Cluster Collaboration (Kenyon et al. 2005; Mayne et al. 2007); (23) Cody & Hillenbrand 2010; (24) AAVSO.

(This table is available in its entirety in a machine-readable form in the online journal. A portion is shown here for guidance regarding its form and content.)

in absorption (SO 1123, SO 243, SO 92, and SO 379) have discrepant RV, which causes us to suspect that they are not members of the cluster. Another possibility is that these stars are binaries with variable RVs. Since, the frequency of binaries increases with the stellar mass (e.g., Duchêne & Kraus 2013), the probability to find a binary member with discrepant RV in solar-type stars is higher in comparison with low-mass stars. We labeled these stars as probable members. We rejected as members of the cluster stars with very low (<0.3%) photometric membership probability and stars with discrepant RV that do not have additional features of youth. Finally, some stars do not have enough information to define their membership and were labeled as uncertain members.

For low-mass stars (from K0 to M2.5) and for very low-mass stars (M3 or later), the presence of Li I λ6708 in absorption is a reliable indicator of youth. For very low-mass stars when the presence of Li I λ6708 in absorption is uncertain (flag "1"), we used the measurements of Na I λ8195 to support the membership status. Moreover, stars with uncertain flag of Li I λ6708 that exhibit other indicators to be members of the cluster (including previous Li I λ6708 reported for the star) are also classified as members of the σ Orionis cluster. We also considered member of the cluster stars with protoplanetary disks classified as accretors using the Hα line. Finally, RV can be used as a strong membership criteria for stars in the entire spectral type range and could be use to separate the σ Ori stellar population and the sparser stellar population (see Section 2.3).

Optical spectra and spectral energy distributions (SEDs) for the entire sample with spectral types obtained in Section 3.1, plus additional information compiled from Tables 2, 4, and 6 for each star, is available online.[16] This online tool is a work in progress and we expect to add new objects and to extend the information about the population of the σ Orionis cluster.

Finally, Table 7 compiles membership information for a set of stars studied in high resolution (Section 3.2) but without low-resolution analysis or spectral types (Section 3.1). Our memberships are based on RV criteria, presence of Li I λ6708 in absorption, and the accretion criteria from White & Basri (2003).

4. DISK POPULATION AND ACCRETION

4.1. Revisiting the Disk Census in the Cluster

In H07b, we studied the disk population in the region covered by the four channels of IRAC. Since mosaics of channels 4.5 μm and 8.0 μm have a 6.″5 displacement to the north from the mosaics of channels 3.6 μm and 5.8 μm, the region with the complete IRAC data set is smaller than the field of view of individual IRAC mosaics. MIPS observations in the σ Orionis cluster also cover more area in the north–south direction in comparison to the region covered by the complete IRAC data set. A more detailed description of MIPS and IRAC data can be found in H07b.

We searched for infrared excesses at 24 μm in the newly identified candidates within the photometric sample (Table 2) reanalyzing the MIPS observation of the σ Orionis cluster. We followed the procedure described in Hernández et al. (2007a, 2007b, 2008, 2009, 2010) to identify stars with excess at 24 μm. Figure 10 shows the color–color diagram used to select new disk bearing candidates of the cluster. Photospheric limits (dotted lines) were defined by H07b using the typical K-[24] color of diskless stars detected in the MIPS observation. An arbitrary limit between optically thick disks (II) and debris disks (dashed line) was defined using the K-[24] color of a

[16] http://sigmaori.cida.gob.ve/

Table 7
Membership for Stars without Spectral Types Studied in Section 3.2

Name H07	2massID	Li Flag	Li Ref.	RV Flag	RV Ref.	Hα Flag.	Disk	X-Ray Ref.	PM Flag	Dist Flag	Var Flag	$\%_{pho}$	Member Flag
SO1154	05393982-0233159	0	4	···	···	Y	II	14,19	2	1	21,22,23,24	22.7	M:
SO82	05373187-0245184	0	···	···	···	···	III	···	2	0	···	22.9	U:
SO164	05374491-0229573	0	···	0	···	···	III	14	2	1	···	10.6	N:
SO251	05375512-0227362	2	···	···	···	N	III	19	···	1	···	95.3	M:
SO302	05380167-0225527	0	···	···	···	N	III	16,18,19	···	1	22	74.7	P:
SO304	05380221-0229556	0	···	1	···	···	III	···	1	1	···	33.6	U:
SO329	05380561-0218571	0	···	0	···	···	III	···	···	1	···	0.0	N:
SO371	05380966-0228569	0	···	···	···	···	III	···	···	1	···	0.0	N:
SO424	05381589-0234412	0	···	0	···	···	III	···	2	1	···	3.1	N:
SO482	05382307-0236493	0	···	···	20	Y	II	···	···	1	21,22,23	50.5	M:
SO548	05382995-0215405	0	···	···	···	N	III	···	···	0	24	32.0	U:
SO561	05383138-0255032	0	···	0	···	···	III	···	2	1	···	23.3	N:
SO620	05383654-0233127	0	···	···	···	···	III	···	2	1	···	82.3	U:
SO674	05384159-0230289	2	8	2	8	N	II	···	2	1	21,22	98.2	M:
SO692	05384375-0252427	0	5	···	13,5	N	III	···	···	1	22	32.4	M:
SO738	05384809-0228536	0	5	···	5	N	II	···	···	1	···	66.6	M:
SO773	05385173-0236033	2	8	···	8	N	III	14,15,18,19	···	1	21	31.1	M:
SO797	05385492-0228583	0	5	···	5	N	III	14,19	···	1	···	55.7	M:
SO877	05390524-0233005	0	5,6	···	5	N	III	14,18,19	1	1	22,23	72.2	M:
SO917	05391001-0228116	0	···	···	5	···	EV	···	···	1	···	3.6	M:
SO946	05391447-0228333	0	3	2	8,2	N	III	14,18,19	1	1	22,23	44.5	M:
SO1005	05392097-0230334	0	5	···	5	N	III	14,19	···	1	21,22,23	4.9	M:
SO1043	05392561-0234042	2	···	···	···	N	III	···	···	1	21,23	49.0	M:
SO1057	05392677-0242583	0	6	···	···	···	EV	19	···	1	22,23	8.1	M:
SO1370	05401304-0228314	0	···	···	···	···	III	···	···	0	···	0.0	N:

Notes.
Disk type: III = diskless, II = thick disk, I = class I, EV = evolved disk, TD = transition disk, DD = Debris disk. Member-flag: M: member, N: non-member, U: uncertain, P: probable member, U: uncertain member.
References. (1) Zapatero Osorio et al. 2002; (2) Barrado y Navascués et al. 2003; (3) Andrews et al. 2004; (4) Kenyon et al. 2005; (5) Caballero 2006; (6) Sacco et al. 2008; (7) Maxted et al. 2008; (8) Caballero 2008a; (9) Skinner et al. 2008; (10) López-Santiago & Caballero 2008; (11) Caballero 2010; (12) XMM-SSC, 2010); (13) Burningham et al. 2005; (14) CVS; (15) Cluster Collaboration (Kenyon et al. 2005; Mayne et al. 2007); (16) Cody & Hillenbrand 2010; (17) AAVSO.

Table 8
New Photometric Candidates with Infrared Excess at 24 μm

Name	2massID	V (mag)	[3.6] (mag)	[4.5] (mag)	[5.8] (mag)	[8.0] (mag)	[24] (mag)	Disk Type
···	05373456-0255588	22.70	···	13.45 ± 0.03	···	12.36 ± 0.04	8.73 ± 0.04	II
SO238	05375398-0249545	18.47	11.11 ± 0.03	10.72 ± 0.03	10.39 ± 0.03	9.79 ± 0.03	7.24 ± 0.03	II
···	05381279-0212266	20.28	12.93 ± 0.03	···	12.30 ± 0.04	···	8.27 ± 0.03	II
···	05382503-0213162	17.44	11.83 ± 0.03	···	11.34 ± 0.03	···	8.39 ± 0.03	II
···	05382656-0212174	15.12	10.18 ± 0.03	···	9.31 ± 0.03	···	6.77 ± 0.03	II
SO595	05383444-0228476	11.30	10.42 ± 0.03	10.29 ± 0.03	10.15 ± 0.03	9.95 ± 0.03	8.27 ± 0.03	DD/EV
···	05383981-0256462	14.62	···	9.31 ± 0.03	···	7.90 ± 0.03	5.05 ± 0.03	II
···	05384714-0257557	21.15	···	12.82 ± 0.03	···	11.55 ± 0.03	8.94 ± 0.04	II
···	05392639-0215034	14.51	9.33 ± 0.03	···	8.38 ± 0.03	···	4.18 ± 0.03	II
SO1084	05393136-0252522	12.50	10.70 ± 0.03	10.77 ± 0.03	10.74 ± 0.03	10.68 ± 0.03	9.88 ± 0.06	DD/EV
···	05394097-0216243	18.01	11.05 ± 0.03	···	10.32 ± 0.03	···	7.57 ± 0.03	II
···	05394278-0258539	14.25	···	8.97 ± 0.03	···	7.75 ± 0.03	4.43 ± 0.03	II
SO1340	05400477-0245245	18.87	12.87 ± 0.04	12.83 ± 0.04	12.63 ± 0.05	11.51 ± 0.04	9.13 ± 0.04	II [a]
···	05400676-0257389	18.67	···	···	···	···	9.58 ± 0.05	II[a]

Notes.
Disk type: II = thick disk, DD/EV = debris disks or evolved disk.
[a] Potential galaxies based on the profile classification of UKIDSS.

sample of known debris disks located in several young stellar groups (Hernandez et al. 2011). Open squares represent stars not included in the previous MIPS analysis (H07b). Out of 14 new disk bearing candidates, 12 have 24 μm infrared excess expected in stars with optically thick disks. The remaining two stars show 24 μm expected in stars with debris or evolved disks (K-24 $\lesssim$ 3.0; Hernandez et al. 2011). Two disk bearing candidates are potential galaxies based on the profile classification of UKIDSS (red X's). *Spitzer* photometry and disk type for each source are provided in Table 8.

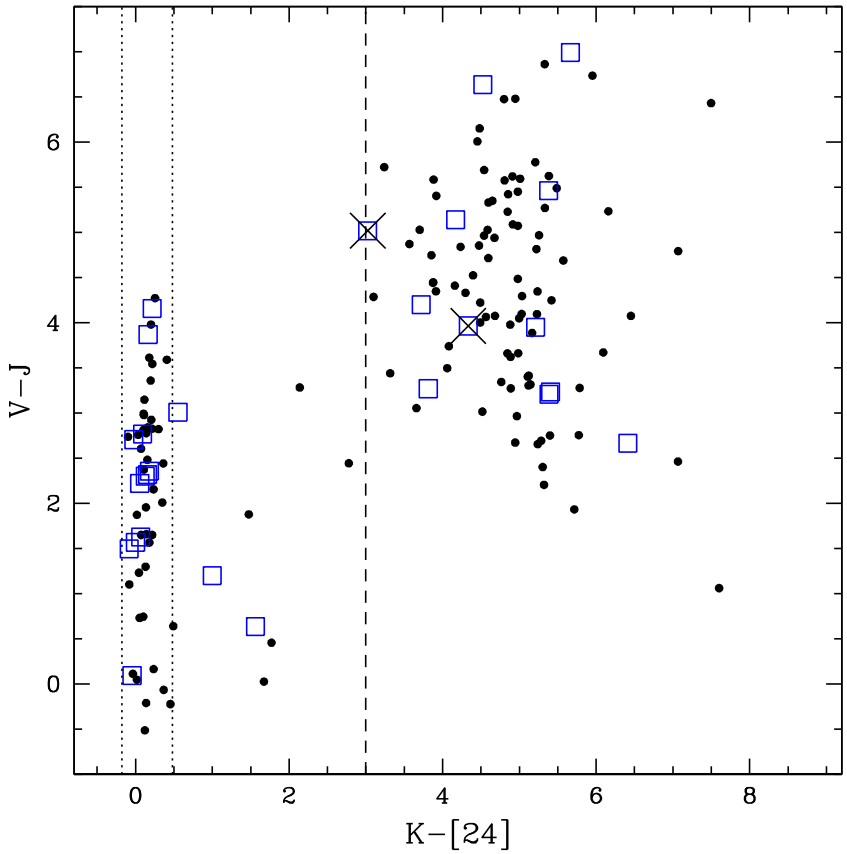

Figure 10. Color–magnitude diagram K-24 versus $V-J$ illustrating the detection of disks at 24 μm. Circles and squares represent sources included and not included in the previous disk census (H07b), respectively. Dotted lines represent the photospheric K-24 colors estimated by H07b. The dashed line indicates an arbitrary limit between optically thick disks and debris disks estimated using a sample of debris disks located in several young stellar groups (Hernandez et al. 2011). Red X's are sources labeled as galaxies by Lawrence et al. (2013).

(A color version of this figure is available in the online journal.)

4.2. Disk Emission and Accretion Indicators

Independently of the spectral type, WH_α_10% is an indicator of accretion (White & Basri 2003; Jayawardhana et al. 2003). Studying very low-mass young objects, Natta et al. (2004) found that WH_α_10% can be used to roughly estimate accretion rates ($\dot{M}_{\rm acc}$). The relation of $\dot{M}_{\rm acc}$ as a function of WH_α_10% from Natta et al. (2004) indicates that stars accreting below the detectable level have $\log(\dot{M}_{\rm acc}) \lesssim -10.3\ M_\odot\ {\rm yr}^{-1}$ and $\log(\dot{M}_{\rm acc}) \lesssim -11\ M_\odot\ {\rm yr}^{-1}$ for the accretion cutoff of 270 km s^{-1} (White & Basri 2003) and 200 km s^{-1} (Jayawardhana et al. 2003), respectively, although a large chromospheric contamination is expected if the mass accretion rates have such low levels (Ingleby et al. 2011).

Figure 11 shows the relation between the WH_α_10% versus the IRAC SED slope determined from the [3.6]–[8.0] color. The horizontal solid line indicates the limit between optically thick disks and evolved disk objects based on their infrared excess at 8 μm (Lada et al. 2006; H07b). We plotted stars with optically thick disks (open circles), evolved disks (open squares), and TDs (open triangles) from H07b. In general, diskless stars have WH_α_10% $<$ 270 km s^{-1}, which is the accretion cutoff proposed by White & Basri (2003). We found eight objects with infrared excess at 8 μm consistent with optically thick disks but that are not accreting or are accreting below the detectable level (hereafter very slow accretor). These stars are SO 467, SO 738, SO 435, SO 674, SO 451, SO 247, SO 697, and SO 662. The star SO 823 was also included as a very slow accretor candidate. This star has a strong absorption component at Hα, we were unable to measure WH_α_10% and thus it was not included in Figure 11. On the other hand, low-resolution spectra of SO 823 shows a single emission Hα profile, which suggests variability in the profile of Hα. Additionally, photometric measurements from CVSO indicate that SO 823 is a variable star with amplitude of $\Delta V \sim 2.5$ mag. Objects such as UX Ori-type and AA Tau-type show photometric and spectroscopic variability in which Hα could change from single emission line profile to a profile with a strong central absorption component.

Figure 12 shows the distribution on the IRAC color–color diagram ([5.8]–[8.0] versus [3.6]–[4.5]) for stars studied in Figure 11. The very slow accretor candidates (including the star SO 823) were plotted with solid circles. Stars with optically thick disks classified as accretor and very slow accretor candidates fall in similar region in this plot. Thus, very slow accretors candidates have similar infrared excesses in the IRAC bands in comparison with stars with optically thick disks classified as accretors using the accretion cutoff proposed by White & Basri (2003).

Low-resolution spectroscopic analysis (Section 3.1) supports the low accretion level for stars SO 823, SO 467, SO 435, and SO 451. Moreover, in Figure 3, we can identify four additional very low accretor candidates (SO 566, SO 598, SO 682, and SO 967) bearing optically thick disks that were classified as non-accretor following the criteria from Barrado y Navascués et al. (2003). High-resolution studies are necessary to determine

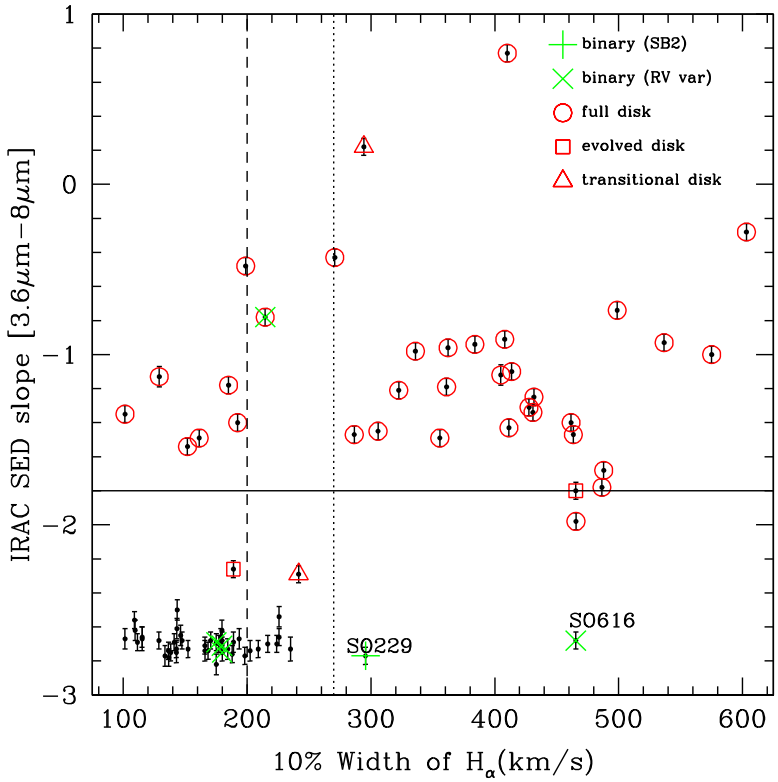

Figure 11. IRAC SED slope versus the full width of H_α at 10% of the line peak. Dotted line and dashed line represent the limit between accretor and non-accretor from White & Basri (2003) and Jayawardhana et al. (2003), respectively. Solid line indicates the limit between optically thick disks and evolved disks (Lada et al. 2006). Other symbols are similar to Figure 7. The diskless stars SO 299 and SO 616 can be binaries or fast rotators (see Figure 14). We identify eight very slow accretors with optically thick disks. We also identify one transitional disk (SO 818) and one evolved disk (SO 905) with accretion below the measurable levels.

(A color version of this figure is available in the online journal.)

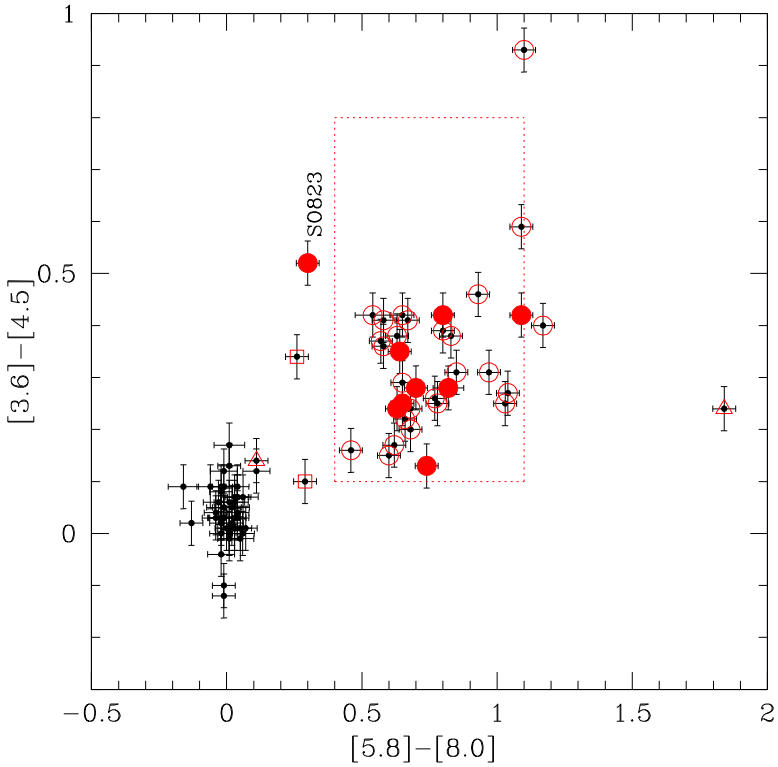

Figure 12. IRAC color–color diagram [5.8]–[8.0] vs. [3.6]–[4.5] for stars included in Figure 11. Solid circles represent the very slow accretors candidates. We also included in this plot the slow accretors candidate SO 823. The large dotted box represents the loci of classical T Tauri stars (CTTSs) with different accretion rates (D'Alessio et al. 2006). Very slow accretors, candidates, and stars with optically thick disks (Class II) that are above the accretion cutoff (White & Basri 2003) share the same region in this plot. Symbols are similar to Figure 11.

(A color version of this figure is available in the online journal.)

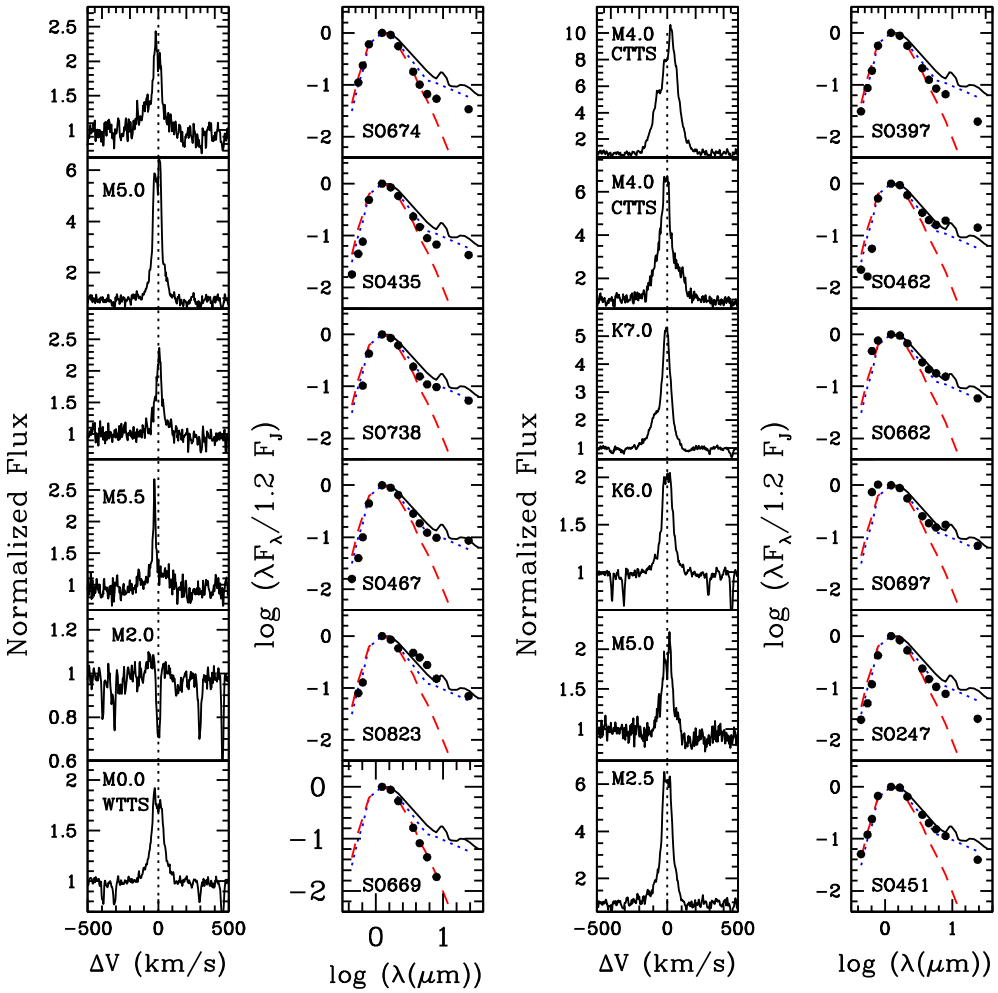

Figure 13. Spectral energy distributions (SEDs) and H_α profiles for stars identified as very slow accretor candidates. For comparison, we include a diskless star (SO 669) and two stars with accretion disks (SO 397 and SO 462). All SEDs are normalized at the *J* band. Values of the WH_α_10% in km s^{-1} are included in the panels that show the profile of H_α. We do not measure the WH_α_10% of the star SO 823, which exhibits a strong absorption component in the H_α line. In the panels that show the SEDs, we plot the median SED for Class II stars in Taurus (Furlan et al. 2006, solid lines), the median SED for Class II (dotted lines), and the median SED for Class III (dashed lines) in the σ Orionis cluster (H07b).

(A color version of this figure is available in the online journal.)

whether these stars are accreting or not (e.g., Espaillat et al. 2008; Ingleby et al. 2011).

Figure 13 shows normalized SEDs and H_α profiles of the very slow accretor candidates detected in our high-resolution spectra. For comparison, we show SEDs and profiles of a diskless star (SO 669) and two stars classified as accretor in Figure 11 (SO 397 and SO 462). Particularly, SO 462 has WH_α_10% on the accretion cutoff defined by White & Basri (2003). The star SO 397 exhibits infrared excesses below the median SED for class II stars in the σ Orionis cluster. High inclination of the disk (edge-on) or dust settling could be responsible for the relatively small infrared excesses observed in this star. The star SO 823 has a jump in the SED between the 2MASS and the IRAC measurements, which could be caused by variability or an unresolved binary. Some stars like SO 467, SO 435, SO 451, and SO 462 exhibit asymmetries in the Hα profile that are characteristic of accreting disks. The emission of Hα could have a contribution from the stellar chromosphere or the stars could have variable accretion rate, so the WH_α_10% could vary and would not be a robust quantitative indicator of accretion (e.g., Nguyen et al. 2009a, 2009b). Thus, we need additional studies to understand whether these stars have stopped accreting or if they are in a passive phase in which accretion is temporally stopped or if accretion is below the measurable levels in WH_α_10%. Previous studies have found very low accretors stars in other young stellar populations. Studying the accretion properties in Chameleon I and ρ Oph, Natta et al. (2004) found a population of very low-mass objects with evidence of disks but no detectable accretion activity estimated using several indicators of accretion. Nguyen et al. (2009a) also found a group of stars in Chameleon I (~2 Myr old) with excess at 8 μm and accretion rates below the measurable levels in WH_α_10%. They also found that non-accreting objects with disks do not seem to exist in the Taurus-Auriga star forming region.

On the other hand, Figure 11 shows two diskless stars (SO 616 and SO 229) exhibiting WH_α_10% larger than the accretors limits. One of these stars, SO 229, was identified as a double lined spectroscopic binary from the cross-correlation function while the star SO 616 was recognized as possible binary based on RV variability. These two stars have Li I λ6708 in absorption and spectral types of G2.5 and K7, respectively (see Section 3.1). In Figure 14, we compare the Hectochelle spectra of SO 229 and SO 616 to stars with similar spectral types (G3 for SO 229 and K7 for SO 616). It is apparent that SO 299 and SO 616 have

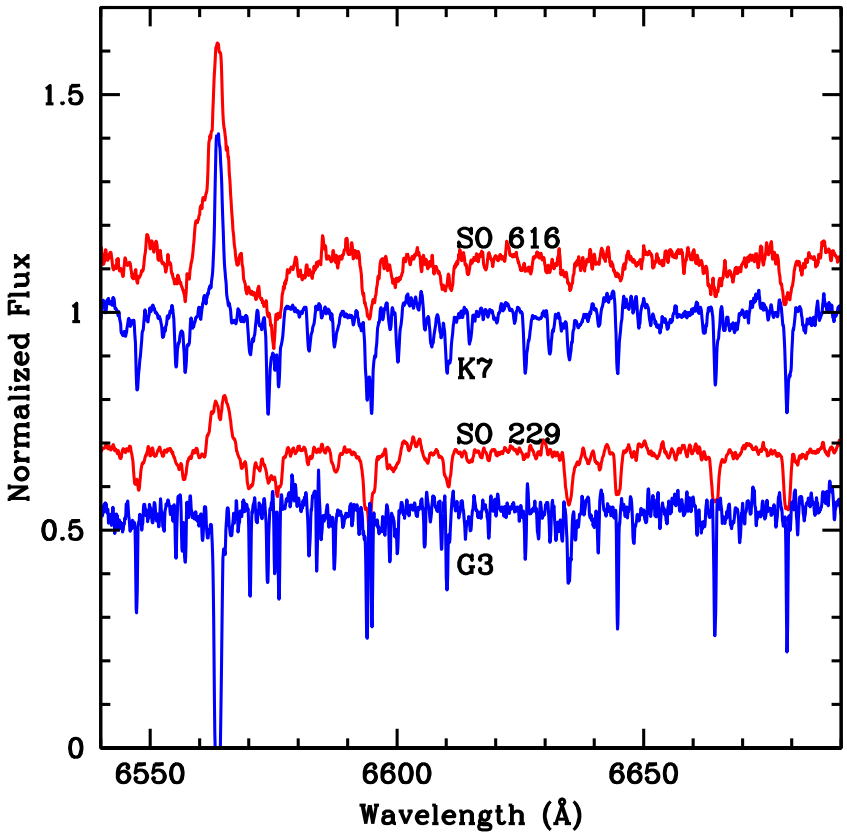

Figure 14. Hectochelle spectra of the diskless stars SO 229 and SO 616 that mimic stars with accretion disks. For comparison, we show hectochelle spectra of diskless stars with similar spectral types. Clearly, SO 229 and SO 616 have wider photospheric features in comparison to those stars. The broader spectral features could be produced by combined spectral lines of stellar components with similar effective temperature or by fast rotation.

(A color version of this figure is available in the online journal.)

wider photospheric features. It is possible that wider spectral features are combined features from components in binary stars with similar spectral types. Another possibility is that the broadening of spectral lines in these objects can be caused by fast rotation. Non-accreting objects with projected rotational velocities larger than ∼50 km s^{-1} can generate WH$_\alpha$_10% > 270 km s^{-1} (see Figure 5 of Jayawardhana et al. 2006). A multi-epoch spectroscopic analysis will help to reveal the nature of these objects.

Low resolution spectroscopic analysis (Section 3.1) shows three diskless stars (SO 229, SO 1123, and SO 1368) that mimic the Hα width expected in stars with accretion disks (see Figure 3). The star SO 299 shows broad photospheric features that could be produced by binarity or fast rotation (Figure 14). The star SO1123 has been classified as spectroscopic binary (Caballero 2007) and fast rotator with a very high projected rotational velocity (Alcalá et al. 2000). The star SO 1368 is a variable star (Mayne et al. 2007) with spectral type K6.5 and still does not have information about multiplicity or rotation. These diskless objects with Hα in emission could have substantial contribution produced by strong chromospheric activity related to fast rotation.

5. SUMMARY AND CONCLUSIONS

Combining 2MASS data (Cutri et al. 2003), new optical photometry obtained with the OSMOS instrument, an updated optical photometry from the CVSO and photometric information from previous work (Sherry et al. 2004; Kenyon et al. 2005; Mayne et al. 2007; Kharchenko & Roeser 2009), we defined a list of photometric candidates of the σ Orionis cluster. Substantial contamination is expected for solar-type stars ($V-J \sim 1.5$) because a branch of field stars cross the PMS population of the cluster in the color–magnitude diagram used to select photometric candidates. A subset of these candidates were characterized using spectroscopic data.

We have applied a consistent spectral classification scheme aimed at PMS stars. The low-resolution spectroscopic data set for spectral typing comes from several instruments with similar spectral coverage and resolution. We were able to determine spectral types for 340 objects located in the general region of the σ Orionis cluster. Analysis of this data set enables us to define membership indicators based on the accretion status obtained from the Hα line (Barrado y Navascués et al. 2003), the presence of Li I λ6708 in absorption (for LMS and for VLMS), and, for a subset of VLMS observed with the Hectospec instrument, the intensity of the line Na I λ8195. So far, this analysis constitutes the largest homogeneous spectroscopic characterization of members in the σ Orionis. Additionally, we were able to determine RVs for 95 stars out of a total sample of 142 objects observed at high resolution in the general region of the cluster. For this high-resolution spectroscopic data set, we also determined membership indicators based on the presence of Li I λ6708 in absorption and the width of the Hα line (White & Basri 2003). The RV distribution for members of the cluster is in agreement with previous works (e.g., Sacco et al. 2008; Maxted et al. 2008; González Hernández et al. 2008).

We have identified and assigned spectral types to 178 bona-fide members of the σ Orionis cluster, combining results from our spectroscopic analysis, previous membership (based on

Table 9
Known Members Compiled in Section 2.3 and New Disk Bearing Candidates not Listed in Tables 6 and 7

Name H07	2massID	V (mag)	Disk Type	Li Ref.	RV Ref.	X-ray Ref.	PM Flag	Dist Flag	Var Ref.	$\%_{pho}$	Spectral Type	SpT Ref.	Notes
···	05401308-0230531	9.213	···	···	···	···	2	0	···	17.1	B9.5,B9.5	32,33	[b]
SO164	05374491-0229573	10.946	III	···	···	14	2	1	···	10.6	G9.0	14	
SO1084	05393136-0252522	12.500	EV/DD	···	···	···	1	0	···	0.0	···	···	[d]
···	05400365-0216461	14.946	···	6	···	···	2	0	22	74.7	···	···	
SO663	05384053-0233275	17.649	II	8	8,13	···	···	1	21	32.8	M4.0	8	
SO1238	05395056-0234137	18.394	III	5	5,13	···	···	1	22,23	68.2	M3.5	29	
···	05394299-0213333	18.580	···	5	···	···	···	0	···	44.4	M4.0	29	
SO976	05391699-0241171	18.862	III	···	···	14,18,19	···	1	22,23	15.0	···	···	
SO1005	05392097-0230334	19.255	III	5	···	14,19	···	1	21,22,23	4.9	M5.0	29	
SO762	05385060-0242429	19.418	II	5	5,13	···	···	1	22	52.4	M4,M5	29,30	
SO767	05385100-0249140	20.040	III	5	5	···	···	1	···	6.9	M4.5	29	
SO1019	05392319-0246557	21.060	III	5	···	···	···	1	···	25.3	M5.5	9	
···	05374557-0229585	···	···	6	···	···	2	1	···	0.0	···	···	[c]
SO1215	05394741-0226162	···	III	···	···	18	2	1	···	0.0	···	···	[c]

Notes.
Disk type: III = diskless, II = thick disk, I = class I, EV= evolved disk, TD = transition disk, DD = Debris disk.
[a] Source labeled as galaxy by Lawrence et al. (2013).
[b] Bright member of the cluster (Sherry et al. 2008; Caballero 2007).
[c] Photometric candidate (Lodieu et al. 2009).
[d] New disk bearing candidate (Section 4.1).
References. (1) Wolk 1996; (2) Zapatero Osorio et al. 2002; (3) Barrado y Navascués et al. 2003; (4) Andrews et al. 2004; (5) Kenyon et al. 2005; (6) Caballero 2006; (7) González Hernández et al. 2008; (8) Sacco et al. 2008; (9) Caballero et al. 2012; (12) Muzerolle et al. 2003; (13) Maxted et al. 2008; (14) Caballero 2008a; (15) Skinner et al. 2008; (16) López-Santiago & Caballero 2008; (17) Caballero et al. 2009; (18) Caballero 2010; (19) XMM-SSC, 2010); (20) Burningham et al. 2005; (21) CVSO (Briceño et al. 2005); (22) Cluster Collaboration (Kenyon et al. 2005; Mayne et al. 2007); (23) Cody & Hillenbrand 2010; (24) AAVSO; (25) Béjar et al. 1999; (26) Scholz & Eislöffel 2004; (27) Cody & Hillenbrand 2011; (28) Rigliaco et al. 2012; (29) Oliveira et al. 2006; (30) Gatti et al. 2008; (31) Oliveira & van Loon 2004; (32) Sherry et al. 2008; (33) Houk & Swift 1999.

(This table is available in its entirety in a machine-readable form in the online journal. A portion is shown here for guidance regarding its form and content.)

RV distribution and the presence of Li I λ6708) and other membership indicators like detection of protoplanetary disks, X-ray emission, proper motion criteria, distance from the central star, variability, and photometric membership probability. We also have identified 14 bona-fide members of the cluster using high-resolution analysis and reported membership indicators. Additionally, we have identified and assigned spectral types to 25 probable members of the cluster. Finally, 36 stars do not have enough information to assign membership (uncertain members).

Of particular interest are stars bearing optically thick disks and narrow Hα profiles not expected in stars with accretion disks. Also of interest are objects with no infrared excess and Hα lines that mimic the Hα width expected in stars with accretion disks (maybe because of binarity or fast rotation). Additional multi-epoch observations are necessary to reveal the nature of these objects.

Additional information, the optical spectra, *UBVRI* magnitudes, membership indicators, and SED for each object analyzed in this work are reported online.[17] Information in this Web site is a work in progress and we expect to increase the spectroscopic database and the membership analysis for additional stars in the σ Orionis cluster.

We thank John Tobin for his advice during the reduction and analysis of the Hectochelle data. Thanks to Gail Schaefer and Jonh Monnier for insightful communications about the distance of the σ Orionis cluster. An anonymous referee provided many insightful comments. We thank Cecilia Mateu for providing the updated version of the CVSO catalog. We also thank Nelson Caldwell, Andy Szentgyorgyi, Perry Berlind, Michael Calkins, and Susan Tokarz for their help in obtaining and processing the Hectospec and FAST spectra. We thank the institutions and personnel that support data acquisition at the Observatorio Astronómico Nacional de Llano del Hato (CIDA), the Observatorio Astronómico Nacional at San Pedro Martir (UNAM), the Observatorio Astrofísico Guillermo Haro (INAOE), and the MDM Observatory (University of Michigan). This publication makes use of data products from the CIDA Equatorial Variability Survey, obtained with the J. Stock telescope at the Venezuela National Astronomical Observatory, which is operated by CIDA for the Ministerio del Poder Popular para Ciencia, Tecnología e Innovación of Venezuela. We also make use of data products from UKIDSS (obtained as part of the UKIRT Infrared Deep Sky Survey) and from the Two Micron All Sky Survey, which is a joint project of the University of Massachusetts and the Infrared Processing and Analysis Center/California Institute of Technology. This work makes use of observations made with the *Spitzer Space Telescope* (GO-1 0037 and GO-1 0058), which is operated by the Jet Propulsion Laboratory, California Institute of Technology, under a contract with NASA. Support for this work was provided by CIDA, the University of Michigan, and by grant UNAM-DGAPA IN109311.

APPENDIX

KNOWN MEMBERS, NEW DISK-BEARING CANDIDATES, AND PHOTOMETRIC CANDIDATES NOT LISTED IN TABLES 6 AND 7

Table 9 includes known members compiled in Section 2.3 and new disk-bearing candidates identified in Section 4.1

[17] http://sigmaori.cida.gob.ve/

Table 10
Additional Photometric Candidates not Listed in Tables 6, 7, and 9

Name H07	2massID	V (mag)	PM Flag	Dist Flag	Var Ref.	$\%_{pho}$	Spectral Type	SpT Ref.
...	05372067-0249330	10.338	0	0	...	71.8	G0	34
...	05401245-0252576	10.494	1	0	...	89.6	F8	34
SO168	05374536-0244124	10.659	0	1	...	88.6	G0	34
...	05375781-0226335	10.744	0	1	...	33.0	G0	34
...	05371881-0231364	10.847	0	0	...	56.8	G0	34
SO1224	05394891-0229110	17.34	...	1	21,23	39.1	...	... [a]
...	05402081-0224003	24.77	...	0	...	50.9	...	...
SO1163	05394057-0225468	...	1	1	...	...	F2	6,34
...	05385382-0244588	...	...	1	...	...	...	... [b]
SO1141	05393816-0245524	...	...	1	...	...	...	... [b]

Notes.
[a] Source labeled as galaxy by Lawrence et al. (2013).
[b] Photometric candidate (Lodieu et al. 2009).
References. (3) Barrado y Navascués et al. 2003; (6) Caballero 2006; (21) CVSO (Briceño et al. 2005); (22) Cluster Collaboration (Kenyon et al. 2005; Mayne et al. 2007); (23) Cody & Hillenbrand 2010; (24) AAVSO; (29) Oliveira et al. 2006; (34) Nesterov et al. 1995.

(This table is available in its entirety in a machine-readable form in the online journal. A portion is shown here for guidance regarding its form and content.)

that were not studied in Sections 3.1 and 3.2. Except for stars observed using the Hectospec and Hectochelle multifiber spectrographs, our target selection includes stars with $V < 16.5$ ($M_* > 0.35\ M_\odot$; see Section 2.5). Out of 125 stars included in Table 9, 107 stars (85.6%) are fainter than our target selection limit. Out of 18 stars with $V < 16.5$, three stars are new disk- bearing candidates. Sorted by optical brightness, Table 9 shows in Columns 1 and 2 source designations from H07b and Cutri et al. (2003), respectively. Column 3 shows visual magnitudes (Section 2.1). Membership information based on the presence of protoplanetary disks, the presence of Li I λ6708, RV measurements, X-ray emission, proper motion, distance from the center of the cluster, and variability are in Columns 4, 5, 6, 7, 8, 9, and 10, respectively. Column 11 gives the photometric membership probability calculated in Section 3.3.1. Spectral types and references are in Columns 11 and 12, respectively.

Sorted by optical brightness, Table 10 includes additional photometric candidates with photometric membership probability higher than ∼32% (within the dashed lines in Figure 8). In these tables, we also include photometric candidates selected by Lodieu et al. (2009; UKIDSS candidates), which are brighter than the completeness limit of 2MASS catalog ($J \sim 15.8$). Out of 11 UKIDSS candidates not included in Table 6, 4 UKIDSS candidates were included in Table 9. The remaining seven stars are listed in Table 10.

REFERENCES

Alcalá, J. M., Covino, E., Torres, G., et al. 2000, A&A, 353, 186
Alcalá, J. M., Terranegra, L., Wichmann, R., et al. 1996, A&AS, 119, 7
Andrews, S. M., Reipurth, B., Bally, J., & Heathcote, S. R. 2004, ApJ, 606, 353
Baltay, C., Snyder, J. A., Andrews, P., et al. 2002, PASP, 114, 780
Barrado y Navascués, D., Béjar, V. J. S., Mundt, R., et al. 2003, A&A, 404, 171
Béjar, V. J. S., Zapatero Osorio, M. R., & Rebolo, R. 1999, ApJ, 521, 671
Béjar, V. J. S., Zapatero Osorio, M. R., & Rebolo, R. 2004, AN, 325, 705
Béjar, V. J. S., Zapatero Osorio, M. R., Rebolo, R., et al. 2011, ApJ, 743, 64
Bell, C. P. M., Naylor, T., Mayne, N. J., Jeffries, R. D., & Littlefair, S. P. 2013, MNRAS, 434, 806
Briceño, C., Calvet, N., Hernández, J., et al. 2005, AJ, 129, 907
Briceño, C., Hartmann, L., Hernández, J., et al. 2007, ApJ, 661, 1119
Briceno, C., Hartmann, L. W., Stauffer, J. R., et al. 1997, AJ, 113, 740
Briceño, C., Vivas, A. K., Calvet, N., et al. 2001, Sci, 291, 93
Brown, A. G. A., de Geus, E. J., & de Zeeuw, P. T. 1994, A&A, 289, 101
Brown, A. G. A., Walter, F. M., & Blaauw, A. 1998, arXiv:astro-ph/9802054
Burningham, B., Naylor, T., Littlefair, S. P., & Jeffries, R. D. 2005, MNRAS, 356, 1583
Caballero, J. A. 2006, PhD thesis, Universidad de La Laguna
Caballero, J. A. 2007, A&A, 466, 917
Caballero, J. A. 2008a, A&A, 478, 667
Caballero, J. A. 2008b, MNRAS, 383, 375
Caballero, J. A. 2008c, MNRAS, 383, 750
Caballero, J. A. 2010, A&A, 514, A18
Caballero, J. A., Albacete-Colombo, J. F., & López-Santiago, J. 2010, A&A, 521, A45
Caballero, J. A., Cabrera-Lavers, A., García-Álvarez, D., & Pascual, S. 2012, A&A, 546, A59
Caballero, J. A., López-Santiago, J., de Castro, E., & Cornide, M. 2009, AJ, 137, 5012
Caballero, J. A., Martín, E. L., Dobbie, P. D., & Barrado Y Navascués, D. 2006, A&A, 460, 635
Caballero, J. A., Valdivielso, L., Martín, E. L., et al. 2008, A&A, 491, 515
Calvet, N., Briceño, C., Hernández, J., et al. 2005, AJ, 129, 935
Cardelli, J. A., Clayton, G. C., & Mathis, J. S. 1989, ApJ, 345, 245
Cody, A. M., & Hillenbrand, L. A. 2010, ApJS, 191, 389
Cody, A. M., & Hillenbrand, L. A. 2011, ApJ, 741, 9
Coelho, P., Barbuy, B., Meléndez, J., Schiavon, R. P., & Castilho, B. V. 2005, A&A, 443, 735
Cohen, M., & Kuhi, L. V. 1979, ApJS, 41, 743
Cunha, K., Smith, V. V., & Lambert, D. L. 1998, ApJ, 493, 195
Cutri, R. M., Skrutskie, M. F., van Dyk, S., et al. 2003, yCat, 2246, 0
D'Alessio, P., Calvet, N., Hartmann, L., Franco-Hernández, R., & Servín, H. 2006, ApJ, 638, 314
Downes, J. J., Briceño, C., Hernández, J., et al. 2008, AJ, 136, 51
Duchêne, G., & Kraus, A. 2013, ARA&A, 51, 269
Espaillat, C., Muzerolle, J., Hernández, J., et al. 2008, ApJL, 689, L145
Fabricant, D., Cheimets, P., Caldwell, N., & Geary, J. 1998, PASP, 110, 79
Fabricant, D., Fata, R., Roll, J., et al. 2005, PASP, 117, 1411
Fazio, G. G., Ashby, M. L. N., Barmby, P., et al. 2004, ApJS, 154, 39
Franciosini, E., Pallavicini, R., & Sanz-Forcada, J. 2006, A&A, 446, 501
Fűrész, G., Hartmann, L. W., Megeath, S. T., Szentgyorgyi, A. H., & Hamden, E. T. 2008, ApJ, 676, 1109
Furlan, E., Hartmann, L., Calvet, N., et al. 2006, ApJS, 165, 568
Garrison, R. F. 1967, PASP, 79, 433
Gatti, T., Natta, A., Randich, S., Testi, L., & Sacco, G. 2008, A&A, 481, 423
González Hernández, J. I., Caballero, J. A., Rebolo, R., et al. 2008, A&A, 490, 1135
Hartmann, L., Calvet, N., Gullbring, E., & D'Alessio, P. 1998, ApJ, 495, 385
Herbst, W., Herbst, D. K., Grossman, E. J., & Weinstein, D. 1994, AJ, 108, 1906
Hernández, J., Calvet, N., Briceño, C., Hartmann, L., & Berlind, P. 2004, AJ, 127, 1682

Hernández, J., Calvet, N., Briceo, C., et al. 2007a, ApJ, 671, 1784
Hernández, J., Calvet, N., Hartmann, L., et al. 2005, AJ, 129, 856
Hernández, J., Calvet, N., Hartmann, L., et al. 2009, ApJ, 707, 705
Hernandez, J., Calvet, N., Hartmann, L., et al. 2011, RMxAC, 40, 243
Hernández, J., Hartmann, L., Calvet, N., et al. 2008, ApJ, 686, 1195
Hernández, J., Hartmann, L., Megeath, T., et al. 2007b, ApJ, 662, 1067
Hernández, J., Morales-Calderon, M., Calvet, N., et al. 2010, ApJ, 722, 1226
Houk, N., & Swift, C. (ed.) 1999, Michigan Catalogue of Two-dimensional Spectral Types for the HD Stars, Vol. 5 (Ann Arbor, MI: Department of Astronomy, University of Michigan)
Hsu, W.-H., Hartmann, L., Allen, L., et al. 2012, ApJ, 752, 59
Ingleby, L., Calvet, N., Bergin, E., et al. 2011, ApJ, 743, 105
Jayawardhana, R., Coffey, J., Scholz, A., Brandeker, A., & van Kerkwijk, M. H. 2006, ApJ, 648, 1206
Jayawardhana, R., Mohanty, S., & Basri, G. 2003, ApJ, 592, 282
Jeffries, R. D., Maxted, P. F. L., Oliveira, J. M., & Naylor, T. 2006, MNRAS, 371, L6
Kenyon, M. J., Jeffries, R. D., Naylor, T., Oliveira, J. M., & Maxted, P. F. L. 2005, MNRAS, 356, 89
Kenyon, S. J., & Hartmann, L. 1995, ApJS, 101, 117
Kharchenko, N. V., Piskunov, A. E., Röser, S., Schilbach, E., & Scholz, R.-D. 2005, A&A, 438, 1163
Kharchenko, N. V., & Roeser, S. 2009, yCat, 1280, 0
Kharchenko, N. V., Scholz, R.-D., Piskunov, A. E., Röser, S., & Schilbach, E. 2007, AN, 328, 889
Lada, C. J., Muench, A. A., Luhman, K. L., et al. 2006, AJ, 131, 1574
Landolt, A. U. 1992, AJ, 104, 340
Landolt, A. U. 2009, AJ, 137, 4186
Lawrence, A., Warren, S. J., Almaini, O., et al. 2007, MNRAS, 379, 1599
Lawrence, A., Warren, S. J., Almaini, O., et al. 2013, yCat, 2319, 0
Lodieu, N., Zapatero Osorio, M. R., Rebolo, R., Martín, E. L., & Hambly, N. C. 2009, A&A, 505, 1115
López-Santiago, J., & Caballero, J. A. 2008, A&A, 491, 961
Luhman, K. L., Hernández, J., Downes, J. J., Hartmann, L., & Briceño, C. 2008, ApJ, 688, 362
Martini, P., Stoll, R., Derwent, M. A., et al. 2011, PASP, 123, 187
Mateu, C., Vivas, A. K., Downes, J. J., et al. 2012, MNRAS, 427, 3374
Maxted, P. F. L., Jeffries, R. D., Oliveira, J. M., Naylor, T., & Jackson, R. J. 2008, MNRAS, 385, 2210
Mayne, N. J., Naylor, T., Littlefair, S. P., Saunders, E. S., & Jeffries, R. D. 2007, MNRAS, 375, 1220
Mink, D. J., & Kurtz, M. J. 1998, in ASP Conf. Ser. 145, Astronomical Data Analysis Software and Systems VII, ed. R. Albrecht, R. N. Hook, & H. A. Bushouse (San Francisco, CA: ASP), 93
Mink, D. J., Wyatt, W. F., Caldwell, N., et al. 2007, in ASP Conf. Ser. 376, Astronomical Data Analysis Software and Systems XVI, ed. R. A. Shaw, F. Hill, & David J. Bell (San Francisco, CA: ASP), 249
Muzerolle, J., Calvet, N., & Hartmann, L. 2001, ApJ, 550, 944
Muzerolle, J., Hillenbrand, L., Calvet, N., Briceño, C., & Hartmann, L. 2003, ApJ, 592, 266
Natta, A., Testi, L., Muzerolle, J., et al. 2004, A&A, 424, 603
Naylor, T. 1998, MNRAS, 296, 339
Naylor, T., Totten, E. J., Jeffries, R. D., et al. 2002, MNRAS, 335, 291
Nazé, Y. 2009, A&A, 506, 1055
Nesterov, V. V., Kuzmin, A. V., Ashimbaeva, N. T., et al. 1995, A&AS, 110, 367
Nguyen, D. C., Jayawardhana, R., van Kerkwijk, M. H., et al. 2009a, ApJ, 695, 1648
Nguyen, D. C., Scholz, A., van Kerkwijk, M. H., Jayawardhana, R., & Brandeker, A. 2009b, ApJL, 694, L153
Oliveira, J. M., Jeffries, R. D., van Loon, J. T., & Rushton, M. T. 2006, MNRAS, 369, 272
Oliveira, J. M., & van Loon, J. T. 2004, A&A, 418, 663
Pecaut, M. J., & Mamajek, E. E. 2013, ApJS, 208, 9
Peña Ramírez, K., Béjar, V. J. S., Zapatero Osorio, M. R., Petr-Gotzens, M. G., & Martín, E. L. 2012, ApJ, 754, 30
Perryman, M. A. C., Lindegren, L., Kovalevsky, J., et al. 1997, A&A, 323, L49
Renson, P., & Manfroid, J. 2009, A&A, 498, 961
Rigliaco, E., Natta, A., Randich, S., Testi, L., & Biazzo, K. 2011, A&A, 525, A47
Rigliaco, E., Natta, A., Testi, L., et al. 2012, A&A, 548, A56
Sacco, G. G., Franciosini, E., Randich, S., & Pallavicini, R. 2008, A&A, 488, 167
Schlieder, J. E., Lépine, S., Rice, E., et al. 2012, AJ, 143, 114
Scholz, A., & Eislöffel, J. 2004, A&A, 419, 249
Scholz, A., Xu, X., Jayawardhana, R., et al. 2009, MNRAS, 398, 873
Sherry, W. H., Walter, F. M., & Wolk, S. J. 2004, AJ, 128, 2316
Sherry, W. H., Walter, F. M., Wolk, S. J., & Adams, N. R. 2008, AJ, 135, 1616
Sicilia-Aguilar, A., Hartmann, L., Calvet, N., et al. 2006, ApJ, 638, 897
Sicilia-Aguilar, A., Hartmann, L. W., Hernández, J., Briceño, C., & Calvet, N. 2005, AJ, 130, 188
Siess, L., Dufour, E., & Forestini, M. 2000, A&A, 358, 593
Simón-Díaz, S., Caballero, J. A., & Lorenzo, J. 2011, ApJ, 742, 55
Skinner, S. L., Sokal, K. R., Cohen, D. H., et al. 2008, ApJ, 683, 796
Stoll, R., Martini, P., Derwent, M. A., et al. 2010, Proc. SPIE, 7735, 77354L
Szentgyorgyi, A., Furesz, G., Cheimets, P., et al. 2011, PASP, 123, 1188
Tobin, J. J., Hartmann, L., Furesz, G., Mateo, M., & Megeath, S. T. 2009, ApJ, 697, 1103
Tonry, J., & Davis, M. 1979, AJ, 84, 1511
Townsend, R. H. D., Oksala, M. E., Cohen, D. H., Owocki, S. P., & ud-Doula, A. 2010, ApJL, 714, L318
Vivas, A. K., Zinn, R., Abad, C., et al. 2004, AJ, 127, 1158
Walter, F. M., Sherry, W. H., Wolk, S. J., & Adams, N. R. 2008, Handbook of Star Forming Regions, Volume I (San Francisco, CA: ASP), 732
Walter, F. M., Wolk, S. J., Freyberg, M., & Schmitt, J. H. M. M. 1997, MmSAI, 68, 1081
Watson, C. L. 2006, JAVSO, 35, 318
White, R. J., & Basri, G. 2003, ApJ, 582, 1109
Williams, J. P., & Cieza, L. A. 2011, ARA&A, 49, 67
Wolk, S. J. 1996, PhD thesis, State Univ. New York at Stony Brook
Zacharias, N., Finch, C. T., Girard, T. M., et al. 2013, AJ, 145, 44
Zapatero Osorio, M. R., Béjar, V. J. S., Pavlenko, Y., et al. 2002, A&A, 384, 937